Department of Applied Physics

Theoretical Description and Design of Optical Nanomaterials

Patrick Grahn

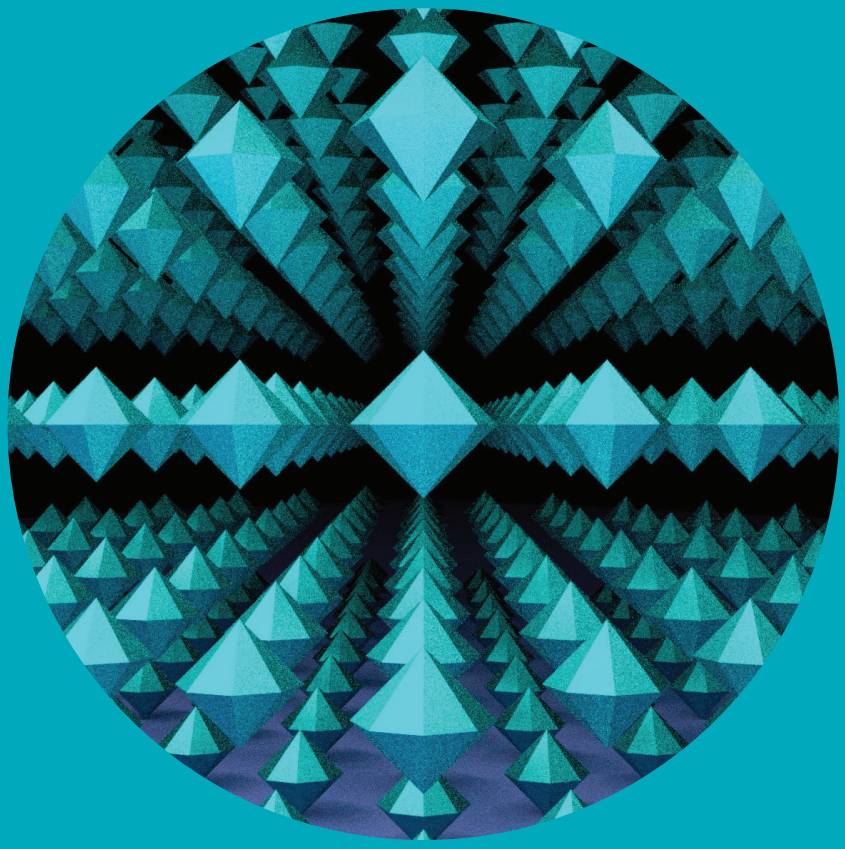

Aalto University

DOCTORAL DISSERTATIONS

Patrick Grahn Theoretical Description and Design of Optical Nanomaterials Aalto University

Aalto University publication series
DOCTORAL DISSERTATIONS 22/2014

Theoretical Description and Design of Optical Nanomaterials

Patrick Grahn

A doctoral dissertation completed for the degree of Doctor of Science in Technology to be defended, with the permission of the Aalto University School of Science, at a public examination held in the Auditorium of the F building (Otakaari 3, Espoo, Finland) on the 11th of April 2014 at 1 p.m.

Aalto University
School of Science
Department of Applied Physics
Optics and Photonics

Supervising professor
Prof. Matti Kaivola

Thesis advisor
Dr. Andriy Shevchenko

Preliminary examiners
Prof. Carsten Rockstuhl, Karlsruhe Institute of Technology, Germany
Prof. Jari Turunen, University of Eastern Finland, Finland

Opponent
Prof. Brian Stout, Institut Fresnel, Aix-Marseille Université, France

Aalto University publication series
DOCTORAL DISSERTATIONS 22/2014

ISBN 978-952-60-5576-3
ISBN 978-952-60-5577-0 (pdf)
ISSN-L 1799-4934
ISSN 1799-4934 (printed)
ISSN 1799-4942 (pdf)
http://urn.fi/URN:ISBN:978-952-60-5577-0

Unigrafia Oy
Helsinki 2014

Finland

441 697
Printed matter

Aalto University

Abstract

Aalto University, P.O. Box 11000, FI-00076 Aalto www.aalto.fi

Author
Patrick Grahn

Name of the doctoral dissertation
Theoretical Description and Design of Optical Nanomaterials

Publisher School of Science

Unit Department of Applied Physics

Series Aalto University publication series DOCTORAL DISSERTATIONS 22/2014

Field of research Nano-optics

Manuscript submitted 17 December 2013 **Date of the defence** 11 April 2014

Permission to publish granted (date) 29 January 2014 **Language** English

☐ **Monograph** ☒ **Article dissertation (summary + original articles)**

Abstract

Recent developments in nanotechnology have made it possible to create a large variety of nanoparticles with predefined shapes. Nanoparticles that are much smaller than the optical wavelengths can appear as artificial atoms to light and, when assembled into a periodic three-dimensional lattice, they form a crystalline optical nanomaterial. The main difference from natural materials is that the optical response of the material can be purposefully tailored by designing the constituting nanoparticles. In fact, optical nanomaterials can exhibit extraordinary optical properties that cannot be found in natural materials. However, in order to successfully design such artificial media, advanced theoretical methods are required.

The main goal of the research described in this thesis was to develop a theoretical basis for a comprehensive treatment of optical nanomaterials. In the developed formalism, the microscopic optical response in the unit cell of a nanomaterial is characterized in terms of elementary electric current multipoles. These multipoles are fundamentally connected to the nanoparticles' geometry, which provides an efficient way to adjust and tune the optical response. The influence of higher-order multipole excitations is demonstrated by designing a nanoscatterer in which light cannot excite any electric dipole moment.

In the thesis, it is shown that the macroscopic optical properties of nanomaterials can straightforwardly be described in terms of the interaction of optical plane waves with the planar arrays of nanoscatterers that compose the medium. Effective material parameters, such as the refractive index and wave impedance, naturally appear in this description in the form of simple analytical expressions. In contrast to existing theories, the introduced approach correctly handles also spatially dispersive materials, including those composed of noncentrosymmetric nanoscatterers. In such materials, two counter-propagating waves can experience the medium differently.

The developed theory reveals the fundamental role of higher-order multipoles and spatial dispersion in realizing extraordinary optical properties with designed nanomaterials. In particular, materials composed of asymmetric nanoparticles may find novel light-guiding and light-harvesting applications. Furthermore, nanomaterials can be designed to suppress optical reflection at certain interfaces only, which can be exploited, e.g., in new interferometric optical devices. Most of the introduced theory can be straightforwardly applied to other artificial media, such as radio-frequency metamaterials and, in some cases, photonic and phononic crystals.

Keywords Optical metamaterials, electromagnetic material parameters, electromagnetic multipoles, spatial dispersion

ISBN (printed) 978-952-60-5576-3 **ISBN (pdf)** 978-952-60-5577-0

ISSN-L 1799-4934 **ISSN (printed)** 1799-4934 **ISSN (pdf)** 1799-4942

Location of publisher Helsinki **Location of printing** Helsinki **Year** 2014

Pages 139 **urn** http://urn.fi/URN:ISBN:978-952-60-5577-0

Aalto-universitetet

Sammandrag

Aalto-universitetet, PB 11000, 00076 Aalto www.aalto.fi

Författare
Patrick Grahn

Doktorsavhandlingens titel
Teoretisk beskrivning och design av optiska nanomaterial

Utgivare Högskolan för teknikvetenskaper

Enhet Institutionen för teknisk fysik

Seriens namn Aalto University publication series DOCTORAL DISSERTATIONS 22/2014

Forskningsområde Nanooptik

Inlämningsdatum för manuskript 17.12.2013 **Datum för disputation** 11.04.2014

Beviljande av publiceringstillstånd (datum) 29.01.2014 **Språk** Engelska

☐ **Monografi** ☒ **Sammanläggningsavhandling (sammandrag plus separata artiklar)**

Sammandrag

Den senaste utvecklingen inom nanoteknologi har gjort det möjligt att producera nanopartiklar med förutbestämd geometrisk form. Nanopartiklar som är mycket mindre än de optiska våglängderna kan framstå som artificiella atomer för ljus. Således kan ett kristallint optiskt nanomaterial bildas genom att ordna dessa partiklar i ett periodiskt tredimensionellt gitter. Till skillnad från naturliga material kan man målmedvetet skräddarsy de optiska egenskaperna hos nanomaterial genom att designa nanopartiklarna. Nanomaterial kan även uppvisa extraordinära optiska egenskaper som inte kan påträffas i naturliga material. För att framgångsrikt designa dessa artificiella medier krävs dock avancerade teoretiska metoder.

Det övergripande målet för forskningen i denna avhandling var att utveckla en teoretisk grund för en utförlig beskrivning av optiska nanomaterial. I den utvecklade formalismen karakteriseras nanomaterialets enhetscells mikroskopiska respons med elementära strömmultipoler. Dessa multipoler är fundamentalt förknippade med nanopartiklarnas geometriska form och således kan nanopartiklarna effektivt justeras för att nå eftertraktade optiska egenskaper. Betydelsen av multipoler av högre ordning demonstreras genom att designa en partikel i vilken ljus inte kan excitera ett elektriskt dipolmoment.

I denna avhandling bevisas att nanomaterials makroskopiska optiska egenskaper kan beskrivas genom växelverkan mellan optiska planvågor och de gitterplan av nanopartiklar som komponerar materialet. Effektiva materialparametrar, som till exempel brytningsindexet och vågimpedansen, framträder naturligt i denna beskrivning i form av enkla analytiska uttryck. I motsatsen till existerande teorier kan den introducerade beskrivningen korrekt hantera också material med spatial dispersion, såsom material komponerade av icke-centrosymmetriska nanopartiklar. I dessa material kan mediet upplevas olikt av två vågor som propagerar i motsatta riktningar.

Den utvecklade teorin avslöjar de fundamentala rollerna av multipoler av högre ordning och spatial dispersion för realiserandet av extraordinära optiska egenskaper med designade nanomaterial. I synnerhet kan material bestående av asymmetriska nanopartiklar potentiellt utnyttjas för styrning och insamling av ljus. Nanomaterial kan även designas till att dämpa reflektion av ljus från enbart specifika gränssnitt, vilket kan utnyttjas för att skapa nya typer av interferometriska optiska instrument. Merparten av den introducerade teorin kan direkt tillämpas på andra artificiella medier såsom radiofrekvensmetamaterial och, i vissa fall, även på fotoniska och fononiska kristaller.

Nyckelord Optiska metamaterial, elektromagnetiska materialparametrar, elektromagnetiska multipoler, spatial dispersion

ISBN (tryckt) 978-952-60-5576-3	**ISBN (pdf)** 978-952-60-5577-0	
ISSN-L 1799-4934	**ISSN (tryckt)** 1799-4934	**ISSN (pdf)** 1799-4942
Utgivningsort Helsingfors	**Tryckort** Helsingfors	**År** 2014
Sidantal 139	**urn** http://urn.fi/URN:ISBN:978-952-60-5577-0	

Preface

The research described in this thesis has been carried out in the Optics and Photonics group in the Department of Applied Physics, Aalto University, during years 2012 and 2013. Within these years, several remarkable findings were made, which are now summarized in this thesis.

First, I wish to express my sincere gratitude to Dr. Andriy Shevchenko for the excellent guidance. He has consistently played an important role in all parts of the research. Furthermore, I am grateful to Prof. Matti Kaivola for introducing me to the world of optics and for supporting my research. I also want to thank all my present and former colleagues at Micronova for the inspiring research environment.

I thank Prof. Brian Stout, for showing interest in my research and for acting as my opponent in the defense of this thesis. I also greatly appreciate the pre-examiners Prof. Carsten Rockstuhl and Prof. Jari Turunen for their timely and careful examination of the thesis.

The research has been funded by the Academy of Finland (Project No. 134029).

Helsinki, January 29, 2014,

Patrick Grahn

Contents

List of publications

This thesis consists of an overview and the following publications which are referred to in the text by their Roman numerals.

I P. Grahn, A. Shevchenko and M. Kaivola. Electromagnetic multipole theory for optical nanomaterials. *New Journal of Physics*, **14**, 093033, September 2012.

II P. Grahn, A. Shevchenko and M. Kaivola. Interferometric description of optical metamaterials. *New Journal of Physics*, **15**, 113044, November 2013.

III P. Grahn, A. Shevchenko and M. Kaivola. Electric dipole-free interaction of visible light with pairs of subwavelength-size silver particles. *Physical Review B*, **86**, 035419, July 2012.

IV P. Grahn, A. Shevchenko and M. Kaivola. Multipole polarizability of a nanodimer in optical waves. *Journal of the European Optical Society - Rapid Publications*, **8**, 13009, January 2013.

V P. Grahn, A. Shevchenko and M. Kaivola. Theoretical description of bifacial optical nanomaterials. *Optics Express*, **21**, 23471–23485, September 2013.

Author's contribution

The author has played a central role in all aspects of the research work. He has developed the theory in Publication I. He proposed the ideas in Publication II and developed the theoretical basis. The nanostructures in Publication III were designed and characterized by the author. The theoretical model in Publication IV was developed by the author. In Publication V, he derived the final equations and performed the design and characterization of the nanomaterial. All numerical calculations were performed by the author. All the articles were prepared by the author.

Other publications to which the author has contributed:

- A. Kravchenko, A. Shevchenko, P. Grahn, V. Ovchinnikov and M. Kaivola, "Photolithographic periodic patterning of gold using azobenzene-functionalized polymers", *Thin Solid Films* **540**, 162–167 (2013).

- A. Kravchenko, A. Shevchenko, V. Ovchinnikov, P. Grahn and M. Kaivola, "Fabrication and characterization of a large-area metal nano-grid wave plate", *Appl. Phys. Lett.* **103**, 033111 (2013).

1. Introduction

"Thus there is no meaning in using the magnetic susceptibility from optical frequencies onward, and in discussing such phenomena we must put $\mu = 1$" reads the famous statement by Landau and Lifshitz [1]. This conclusion is further supported by the fact that all conventional optical materials, natural or artificial, respond essentially only to the electric-field component of light. As a result, the optical response of the materials are fundamentally limited. This prevents optical waves from being manipulated with the same degrees of freedom as radiowaves and microwaves, for which a wide range of practical applications employing magnetic materials exists.

With the advent of nanotechnology, it has become possible to fabricate artificial optical media composed of designed nanoscale scatterers. These scatterers, being smaller in size than the wavelength, appear to light as "artificial atoms". Three-dimensional crystals composed of such scatterers are called optical nanomaterials, which can be considered as a special class of metamaterials. In these artificial materials the properties of optical waves are determined not only by the properties of the constituent materials, but also by the geometrical shape and arrangement of the scatterers. Despite being composed of non-magnetic constituents, artificial nanomaterials can be made magnetic, meaning that their effective optical response yields $\mu \neq 1$. In this way, optical magnetism can be achieved after all. Furthermore, if both the magnetic permeability and electric permittivity can be made simultaneously negative, one can achieve the phenomenon of negative refraction [2].

The horizons of optical nanomaterials are not limited to achieving optical magnetism and negative refraction, but they in general open up a possibility to freely design the optical properties of matter. This potential freedom has inspired investigations into novel optical applications that

cannot be realized using conventional homogeneous materials. Some of the most fascinating applications are perfect imaging [3] and invisibility cloaking [4, 5]. However, in order to actually realize these applications, a reliable and self-consistent theoretical basis enabling one to characterize and design the optical response of nanomaterials must first be developed.

During the last ten years, the research activity on artificial electromagnetic materials has grown enormously. Despite the vast amount of studies performed, the theory describing such materials is still incomplete. For example, artificial atoms are usually described in terms of electric and magnetic dipole moments only. However, in electromagnetic scatterers composed of non-magnetic materials, the magnetic dipole and electric quadrupole are interconnected electric current excitations of the same order and, therefore, they must be considered on equal grounds. This fact has raised the question of possible contributions of electric quadrupoles to the optical response of artificial media [6, 7]. Furthermore, spatial dispersion has been found to be an unavoidable property of such media at optical frequencies [8–11]. In essence, the spatial dispersion implies that the optical characteristics of the individual scatterers and the medium composed of them depend on the light propagation direction. Although one can calculate these characteristics for one propagation direction at a time, the commonly used calculation procedure [12] assumes the same optical properties for waves propagating in different directions. Thus, this and other similar procedures can only be applied to a restricted class of materials composed of highly symmetric nanoscatterers.

One of the main goals of the work presented in the thesis is to tackle the challenges in the design of spatially dispersive optical nanomaterials and develop an accurate theoretical approach to describe them. In the theory developed in this work, higher-order multipole excitations and spatial dispersion are naturally taken into account. These effects are common for optical nanomaterials and can therefore not be excluded from the consideration. The thesis contains examples of nanoscatterers and nanomaterials that are judiciously designed to exhibit particular higher-order multipoles and spatial dispersion. These nanomaterials exhibit optical properties that cannot be obtained in conventional homogeneous media.

The thesis is organized as follows: Chapter 2 presents a theoretical basis for the description of the interaction of optical waves with nanoparticles and planar arrays of such particles. In chapter 3, the concept of designed optical nanomaterials is presented along with a comprehensive theoreti-

cal tool for the characterization of these materials. The application of this tool is demonstrated in chapter 4 by designing various optical nanoscatterers and nanomaterials. Finally, chapter 5 summarizes the obtained results and outlines possible directions for future research.

2. Light interaction with nanoparticles

Light propagating in an optical nanomaterial is repeatedly scattered by the nanoparticles that compose the material. In order to theoretically describe such propagation, it is first necessary to understand the interaction between electromagnetic waves and individual nanoparticles. Thus, this chapter presents the necessary theoretical basis for describing scattering of light by a nanoparticle. Furthermore, the interaction between light and planar arrays of nanoscatterers is also considered.

2.1 Light scattering by a small particle

Nanoparticles are, as the name suggests, solid objects that are smaller than 100 nm in size. These particles are thereby smaller than the wavelength of visible light, which ranges from approximately 380 to 750 nm. It is then clear that the wave nature of light must be taken into account when describing the interaction between light and such particles. This can be done by treating light as a classical electromagnetic field governed by the Maxwell equations.

In matter that is linear and isotropic, time-harmonic electromagnetic fields, oscillating at an angular frequency ω, satisfy the following Maxwell equations [13]

$$\nabla \cdot \big[\varepsilon(\mathbf{r})\mathbf{E}(\mathbf{r})\big] = 0, \tag{2.1}$$

$$\nabla \cdot \big[\mu(\mathbf{r})\mathbf{H}(\mathbf{r})\big] = 0, \tag{2.2}$$

$$\nabla \times \mathbf{E}(\mathbf{r}) = \mathrm{i}\omega\mu(\mathbf{r})\mathbf{H}(\mathbf{r}), \tag{2.3}$$

$$\nabla \times \mathbf{H}(\mathbf{r}) = -\mathrm{i}\omega\varepsilon(\mathbf{r})\mathbf{E}(\mathbf{r}), \tag{2.4}$$

where the electric permittivity ε and magnetic permeability μ are complex-valued material parameters. Here, the $\mathbf{r}$-dependence of ε and μ implies that the space can contain domains of different media. In Eqs. (2.1)-(2.4),

$\mathbf{E}(\mathbf{r})$ and $\mathbf{H}(\mathbf{r})$ are the complex amplitudes of the electric and magnetic fields, respectively. At any location $\mathbf{r}$ and time t, the physical field $\mathbf{E}(\mathbf{r},t)$ is determined by the complex amplitude as

$$\mathbf{E}(\mathbf{r},t) = \mathrm{Re}\{\mathbf{E}(\mathbf{r})e^{-\mathrm{i}\omega t}\}. \tag{2.5}$$

A similar equation holds for the magnetic field $\mathbf{H}(\mathbf{r},t)$.

Inside a homogeneous medium, the material parameters ε and μ are independent of $\mathbf{r}$. However, these material parameters do depend on the frequency of the electromagnetic field. At optical frequencies, the permeability μ is approximately the same as in vacuum, i.e., $\mu \approx \mu_0$. Consequently, the optical properties of a homogeneous material are fully described by ε. Alternatively, one can introduce a refractive index $n = \sqrt{\varepsilon\mu/(\varepsilon_0\mu_0)}$, where ε_0 is the permittivity in vacuum. At optical frequencies, the expression reduces to $n = \sqrt{\varepsilon/\varepsilon_0}$. For many materials, the values of ε or n can be found in the literature [14–19].

Propagation of light in a homogeneous medium is conveniently described in terms of electromagnetic plane waves. A plane wave is a time-harmonic field that satisfies Eqs. (2.1)-(2.4) in an infinite host medium [$\varepsilon(\mathbf{r}) = \varepsilon_\mathrm{h}$, $\mu(\mathbf{r}) = \mu_\mathrm{h}$]. For a plane wave, the complex amplitude of the electric field is

$$\mathbf{E}_\mathrm{pw}(\mathbf{r}) = \mathbf{E}_0 e^{\mathrm{i}\mathbf{k}\cdot\mathbf{r}}, \tag{2.6}$$

where $\mathbf{E}_0$ is a constant vector and the wave vector $\mathbf{k}$ points in the direction of propagation. The length of the wave vector, $k = \omega\sqrt{\varepsilon_\mathrm{h}\mu_\mathrm{h}}$, is called the wave number. The magnetic field $\mathbf{H}_\mathrm{pw}$ can be obtained from Eq. (2.3). More complicated optical fields can always be expressed as linear superpositions of plane waves with different $\mathbf{k}$ and $\mathbf{E}_0$.

In this thesis, elastic scattering of an optical plane wave by nanoparticles is frequently considered. Since the permittivity of a nanoparticle deviates from that of the surroundings, the field cannot be expressed as a plane wave in the vicinity of the nanoparticle. Instead, the electromagnetic field, which satisfies Eqs. (2.1)-(2.4), can be written as a superposition of the incident plane wave and a scattered field as

$$\mathbf{E}(\mathbf{r}) = \mathbf{E}_\mathrm{pw}(\mathbf{r}) + \mathbf{E}_\mathrm{sca}(\mathbf{r}), \tag{2.7}$$

$$\mathbf{H}(\mathbf{r}) = \mathbf{H}_\mathrm{pw}(\mathbf{r}) + \mathbf{H}_\mathrm{sca}(\mathbf{r}). \tag{2.8}$$

Far away from the nanoparticle, the scattered electric field can always be expressed in spherical coordinates in the following form [20]

$$\mathbf{E}_\mathrm{sca}(\mathbf{r}) = \frac{e^{\mathrm{i}kr}}{r}\mathbf{F}(\theta,\phi), \tag{2.9}$$

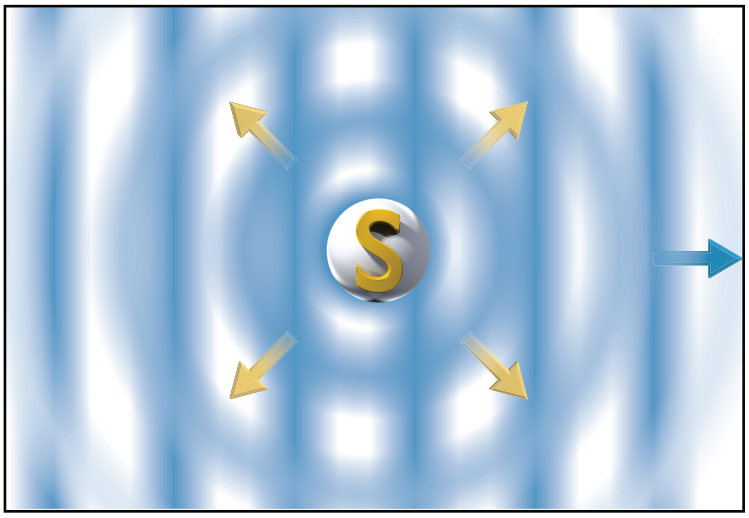

Figure 2.1. Scattering of a time-harmonic plane wave by a small scatterer, S. The wavefronts of the incident and scattered waves at a certain instant of time are shown separately. The scattered far-field is a spherical wave that decays in amplitude as $1/r$ away from the scatterer.

where $r = 0$ is the location of the nanoparticle and $\mathbf{r} \cdot \mathbf{F} = 0$ holds. As illustrated in Fig. 2.1, the total field that satisfies Eqs. (2.1)-(2.4) is a superposition of the incident plane-wave field and a scattered field that decays away from the particle as a spherical wave.

In order to calculate the scattered field for a certain nanoparticle, one must take into account the standard electromagnetic boundary conditions [20]. For a homogeneous spherical scatterer, the scattered field was solved analytically by Lorenz in 1890 [21] and later by Mie in 1908 [22]. The solution involves expanding the scattered field outside the particle, and the total field inside the particle, in vector spherical harmonics [20]. Then, the incident plane wave, with $\mathbf{k} = k\hat{\mathbf{z}}$ and $\mathbf{E}_0 = E_0\hat{\mathbf{x}}$ for example, is written as a superposition of these vector spherical harmonics. Using the electromagnetic boundary conditions, analytical expressions for the expansion coefficients of the scattered field are obtained [13]. Computer codes that can be used to evaluate these coefficients are available [13, 23]. The solution for spherical scatterers can quite straightforwardly be extended to layered spheres, for which computation codes are also available [13, 24]. By employing spheroidal coordinate systems, the scattered field can also be calculated for spheroidal scatterers [25, 26] as well as for layered spheroids [27–29].

For light scattered by geometrically more complicated objects, no simple analytical solutions exist. Fortunately, several numerical techniques [30], such as the finite element method [31] and the finite-difference time-

domain method [32], may be employed on modern computers to solve nearly arbitrary scattering problems. Several commercially available computer softwares [33–43] (and also free ones [44–47]) are particularly suitable for calculating the optical scattering by small particles [48–56]. In the research presented in Publications II-V, we used COMSOL Multiphysics [34] to calculate the scattering properties of nanoparticles and nanoparticle arrays.

Once the field scattered by a particle has been obtained, one can characterize the scatterer by introducing interaction cross sections. These cross sections depend on the characteristics of the field. For a spherical particle they depend only on the excitation frequency ω, but for more complex particles they depend also on the propagation direction and polarization of the incident wave, given by $\mathbf{k}$ and $\mathbf{E}_0$ in Eq. (2.6). One of the interaction cross sections is the scattering cross section C_{sca}. It is equal to the total power scattered by the particle divided by the intensity of the incident wave. It can thereby be interpreted as the area, from which the scatterer takes energy off from the incident light and converts it into scattered light. In analogy, the absorption cross section C_{abs} describes the area from which optical energy is absorbed. The third cross section, coined as the extinction cross section C_{ext}, describes the total effect of both scattering and absorption. The cross sections can be calculated by using the following equations [13]

$$C_{\mathrm{sca}} = \frac{1}{I_0}\int_0^{2\pi}\int_0^{\pi}\frac{1}{2}\mathrm{Re}\{\hat{\mathbf{r}}\cdot[\mathbf{E}_{\mathrm{sca}}(\mathbf{r})\times\mathbf{H}^*_{\mathrm{sca}}(\mathbf{r})]\}r^2\sin\theta\mathrm{d}\theta\mathrm{d}\phi, \tag{2.10}$$

$$\begin{aligned} C_{\mathrm{ext}} = &-\frac{1}{I_0}\int_0^{2\pi}\int_0^{\pi}\frac{1}{2}\mathrm{Re}\{\hat{\mathbf{r}}\cdot[\mathbf{E}_{\mathrm{sca}}(\mathbf{r})\times\mathbf{H}^*_{\mathrm{pw}}(\mathbf{r}) \\ &+\mathbf{E}_{\mathrm{pw}}(\mathbf{r})\times\mathbf{H}^*_{\mathrm{sca}}(\mathbf{r})]\}r^2\sin\theta\mathrm{d}\theta\mathrm{d}\phi, \end{aligned} \tag{2.11}$$

$$C_{\mathrm{abs}} = C_{\mathrm{ext}} - C_{\mathrm{sca}}, \tag{2.12}$$

where $I_0 = \sqrt{\varepsilon_{\mathrm{h}}}|E_0|^2/(2\sqrt{\mu_{\mathrm{h}}})$ is the intensity of the incident plane wave in a non-absorbing host medium. The absorption cross section can also be obtained directly from the electromagnetic power dissipation inside the scatterer as [20]

$$C_{\mathrm{abs}} = \frac{\omega}{2I_0}\int|E(\mathbf{r})|^2\mathrm{Im}\{\varepsilon(\mathbf{r})\}\mathrm{d}^3r. \tag{2.13}$$

Furthermore, an alternative way to calculate C_{ext} is provided by the optical theorem [20]. For a plane wave propagating in the positive z direction ($\mathbf{k} = k\hat{\mathbf{z}}$), C_{ext} can be expressed as

$$C_{\mathrm{ext}} = \frac{4\pi}{k|E_0|^2}\mathrm{Im}\{\mathbf{F}(\theta=0)\cdot\mathbf{E}_0^*\}. \tag{2.14}$$

Equation (2.14) demonstrates the important fact that extinction is caused by the destructive interference between the incident wave and the forward-scattered wave. Using the two different ways to calculate C_{ext} and C_{abs} can serve as a check for the validity of the numerically calculated scattered fields.

2.2 Plasmonic nanoparticles

At optical frequencies, the scattering cross section of a typical dielectric nanoparticle is only a fraction of its largest geometrical cross section. Noble metal nanoparticles, on the other hand, exhibit resonances at which their interaction cross sections can be several times larger than their geometrical cross sections. Let for example a spherical nanoparticle with a diameter of 80 nm and refractive index of 3 (as that of TiO_2 [14]) be located in a medium with a refractive index of 1.5 (SiO_2 [14]). At a vacuum wavelength of $\lambda_0 = 500$ nm, this nanoparticle has a scattering cross section of $C_{\mathrm{sca}} \approx 0.26 C_{\mathrm{geom}}$ (calculated using Ref. [23]), where C_{geom} is the area of the particle's geometrical cross section. If this dielectric sphere is now replaced by a silver sphere of the same size, the scattering cross section increases to $C_{\mathrm{sca}} \approx 8.34 C_{\mathrm{geom}}$ (the refractive index of silver $n_{\mathrm{Ag}} = 0.05 + 3.13\mathrm{i}$ is taken from Ref. [16]). Note that the silver sphere also has a non-zero absorption cross section of $C_{\mathrm{abs}} \approx 0.50 C_{\mathrm{geom}}$ at this wavelength.

The large interaction cross sections of noble metal nanoparticles are due to a resonant coupling of light to collective oscillations of the metal's conduction electrons at the particle's surface [57]. The quantum of this type of electron excitation is called a localized surface plasmon [58]. Because of this, noble metal nanoparticles are often referred to as plasmonic nanoparticles. The applications of plasmonic nanoparticles in science and technology range from enhancement of transition rates of molecules [59,60] to realization of ultrasensitive nanoscale biosensors [61–64]. In Publications II-V, we have used the ability of subwavelength-sized plasmonic nanoparticles to provide strong scattering of light for the creation of nanostructures with new optical functionalities.

The localized surface plasmon resonance (LSPR) in metal nanospheres can be qualitatively explained using a quasi-static model of light-particle interaction. In this model, a spherical particle interacts with a time-harmonic electric field that is assumed to be uniform throughout the volume of the particle. The model thereby approximates the plane-wave scat-

tering in the limit that the wavelength is much larger than the diameter of the sphere. Applying the model, one finds that the electric field scattered by the sphere is equivalent to the near-field of an electric dipole with an electric dipole moment [13]

$$\mathbf{p} = 4\pi\varepsilon_{\mathrm{h}} a^3 \frac{\varepsilon_{\mathrm{np}} - \varepsilon_{\mathrm{h}}}{\varepsilon_{\mathrm{np}} + 2\varepsilon_{\mathrm{h}}} \mathbf{E}_0. \tag{2.15}$$

Here $\mathbf{E}_0$ is the incident electric field, a is the radius of the sphere, and $\varepsilon_{\mathrm{np}}$ and ε_{h} are the electric permittivities of the nanoparticle and the surroundings, respectively. For a typical transparent dielectric host medium at optical frequencies, ε_{h} is a positive number in the range between 1 and 10. Considering a noble metal nanosphere, $\mathrm{Re}\{\varepsilon_{\mathrm{np}}\}$ is a large negative number at infrared wavelengths. This number approaches zero when the wavelength decreases towards the visible spectral range [16]. Thus, for visible light of a certain wavelength one may have $\mathrm{Re}\{\varepsilon_{\mathrm{np}}\} = -2\varepsilon_{\mathrm{h}}$ and, consequently, the denominator in Eq. (2.15) becomes imaginary. This is the LSPR criterion for a small metal sphere. If $\mathrm{Im}\{\varepsilon_{\mathrm{np}}\}$ is small, the dipole moment given by Eq. (2.15) is large at the LSPR, which leads to a large extinction cross section for the particle.

In Fig. 2.2, the extinction cross section of a small gold sphere is depicted as a function of vacuum wavelength λ_0. The LSPR peak in Fig. 2.2 is broadened due to a quite large value of $\mathrm{Im}\{\varepsilon_{\mathrm{np}}\}$ for the shorter wavelengths in the visible spectral range. This is a consequence of the interband transitions in gold atoms [65]. For silver, on the other hand, $\mathrm{Im}\{\varepsilon_{\mathrm{np}}\}$ is relatively small throughout the whole visible spectral range [16], making it a better plasmonic material than gold.

The LSPR wavelength depends strongly on the geometrical shape of the nanoparticle. This behavior can be illustrated by extending the previous quasi-static model to ellipsoidal particles. As shown in Fig. 2.2, the geometry of an ellipsoidal particle is determined by three semiaxes a, b and d. Due to symmetry, the electric field component along each semiaxis excites an electric dipole moment along this axis. Aligning the Cartesian coordinate system as in Fig. 2.2, we can write $\mathbf{p} = \overleftrightarrow{\alpha} \cdot \mathbf{E}_0$, where the polarizability $\overleftrightarrow{\alpha}$ is a diagonal dyadic with elements of the form [13]

$$\alpha_{xx} = 4\pi\varepsilon_{\mathrm{h}} abd \frac{\varepsilon_{\mathrm{np}} - \varepsilon_{\mathrm{h}}}{3\varepsilon_{\mathrm{h}} + 3L_x(\varepsilon_{\mathrm{np}} - \varepsilon_{\mathrm{h}})}. \tag{2.16}$$

Similar expressions hold for α_{yy} and α_{zz}. In Eq. (2.16), the geometrical factor L_x depends on a, b and d [13]. In the case of a spherical particle, $L_x = L_y = L_z = 1/3$ and Eq. (2.16) reduces to Eq. (2.15). For ellipsoids,

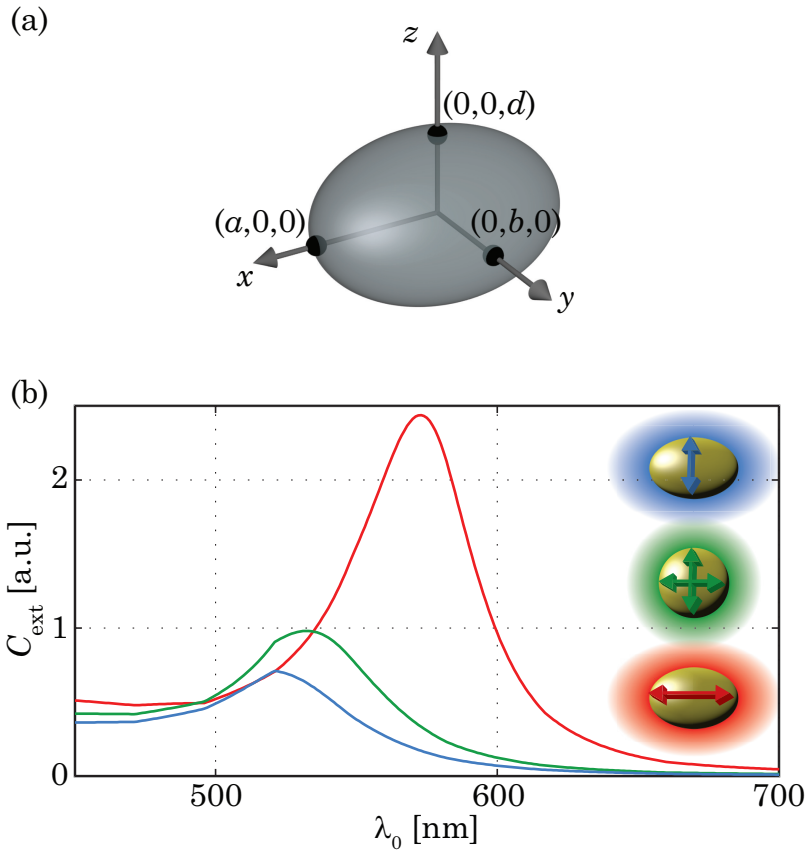

Figure 2.2. (a) Geometry of an ellipsoid ($a \geq b \geq d$). (b) Extinction cross section spectra for gold nanoparticles in the quasi-static limit. In the green curve a spherical nanoparticle (radius a_1) is considered, whereas in the blue and red curves the nanoparticle has a spheroidal shape ($a = 1.3a_1$, $b = d = a_1/\sqrt{1.3}$). For the spheroid, the response to an incident electric field polarized along the x axis and y axis are shown with the red and blue curves, respectively. A host medium with $\epsilon_\mathrm{h} = 2.25\epsilon_0$ is assumed.

there are separate LSPRs for each semiaxis. For example, assuming $a \geq b \geq d$, the geometrical factors obey $L_x \leq L_y \leq L_z < 1$ [13]. Then, the LSPR conditions are $\mathrm{Re}\{\varepsilon_\mathrm{np}\} = -(L_x^{-1} - 1)\varepsilon_\mathrm{h}$ and $\mathrm{Re}\{\varepsilon_\mathrm{np}\} = -(L_y^{-1} - 1)\varepsilon_\mathrm{h}$ for the x- and y-polarized components of the incident field, respectively. As can be seen, a more negative value of $\mathrm{Re}\{\varepsilon_\mathrm{np}\}$ is required to obtain LSPR for x-polarized light. Consequently, the LSPR for this polarization occurs at a longer wavelength than for y-polarized light (see Fig. 2.2).

In Publications II-V, we have considered disc-shaped metal nanoparticles. A disc is geometrically quite close to a prolate spheroid (an ellipsoid with $a = b > d$) and, therefore, the disc can be expected to have only two major resonances. Our nanoscatterer designs rely upon the LSPRs occurring at the longer wavelengths.

The optical properties of plasmonic nanoparticles that are smaller than 10 nm in their effective linear dimensions cannot be accurately described using the electric permittivity of a bulk material. In such particles, the

optical response is affected by the intrinsic size effects such as limitation of the electron mean-free path and quantum confinement [65]. On the other hand, for nanoparticles larger than 10 nm, the electric field of visible light can no longer be assumed to be completely uniform across the volume of the particle. Consequently, the quasi-static model does not yield correct results. Instead, one has to use either exact analytical models for spheroidal scatterers or purely numerical techniques. For larger nanoparticles three new effects appear that are not accounted for by the quasi-static model. First, whereas the extinction of nanoparticles treatable within the quasi-static approximation is dominated by absorption, the extinction of larger particles is dominated by scattering [66] (see also the example in the beginning of this section). Second, the LSPR wavelength shifts towards longer wavelengths with increasing particle size. Finally, the scattered field is no longer electric dipolar, but gets contributions from other electromagnetic multipoles.

2.3 Electromagnetic multipoles

In the previous section, it was noted that in the quasi-static approximation the field scattered by a spheroid is that of a point electric dipole. In general, however, the field scattered by a nanoparticle can be quite different from the electric-dipole field. The scattered field, which depends on the particle shape and composition, is most conveniently described using the electromagnetic multipole expansion. This expansion expresses the field outside the scatterer, in spherical coordinates, as [PI]

$$\mathbf{E}_{\mathrm{sca}}(\mathbf{r}) = E_0 \sum_{l=1}^{\infty} \sum_{m=-l}^{l} \mathrm{i}^l [\pi(2l+1)]^{1/2} \Big\{ \frac{1}{k} a_{\mathrm{E}}(l,m) \nabla \times \big[h_l^{(1)}(kr) \mathbf{X}_{lm}(\theta,\phi) \big] + a_{\mathrm{M}}(l,m) h_l^{(1)}(kr) \mathbf{X}_{lm}(\theta,\phi) \Big\}, \tag{2.17}$$

$$\mathbf{H}_{\mathrm{sca}}(\mathbf{r}) = \frac{E_0}{\eta_{\mathrm{h}}} \sum_{l=1}^{\infty} \sum_{m=-l}^{l} \mathrm{i}^{l-1} [\pi(2l+1)]^{1/2} \Big\{ \frac{1}{k} a_{\mathrm{M}}(l,m) \nabla \times \big[h_l^{(1)}(kr) \mathbf{X}_{lm}(\theta,\phi) \big] + a_{\mathrm{E}}(l,m) h_l^{(1)}(kr) \mathbf{X}_{lm}(\theta,\phi) \Big\}, \tag{2.18}$$

where $\mathbf{X}_{lm}$ are normalized vector spherical harmonics and $h_l^{(1)}$ are spherical Hankel functions of the first kind [20]. The wave number k, wave impedance $\eta_{\mathrm{h}} = \sqrt{\mu_{\mathrm{h}}/\varepsilon_{\mathrm{h}}}$ and electric field amplitude E_0 are parameters describing the incident plane wave in the surrounding host medium. The expansion coefficients $a_{\mathrm{E}}(l,m)$ and $a_{\mathrm{M}}(l,m)$ are the electric and magnetic multipole coefficients, respectively. The integer l describes the order of

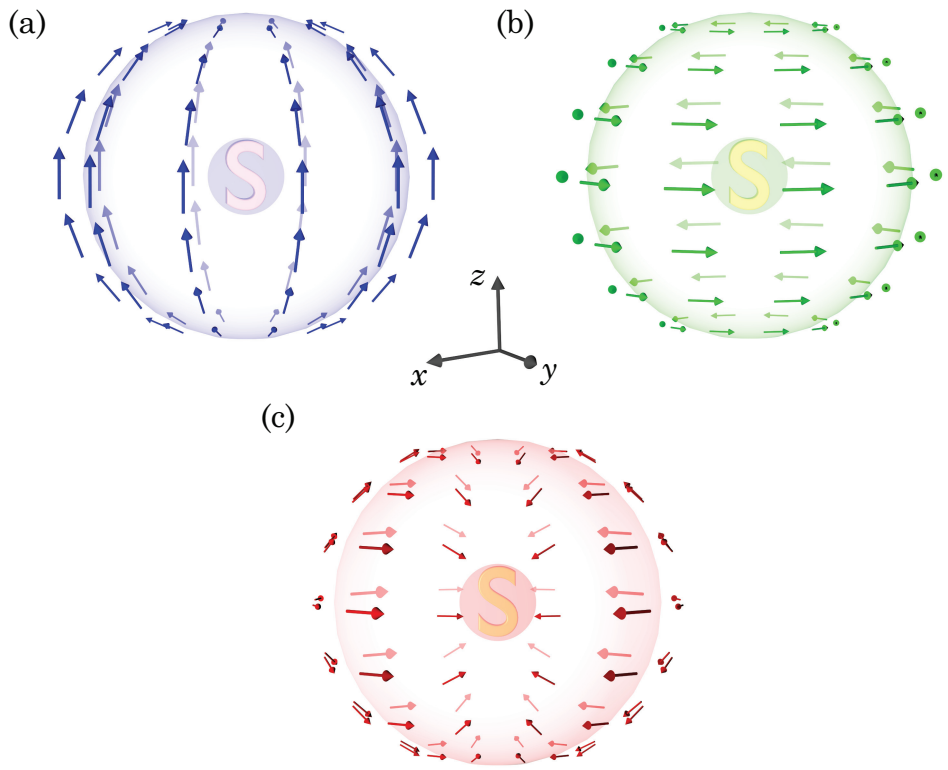

Figure 2.3. Electric far-field distribution $\mathbf{F}(\theta, \phi)$ of (a) a z-polarized electric dipole, (b) a z-polarized magnetic dipole, and (c) an xy-polarized electric quadrupole. The fields are determined by the multipole coefficients (a) $a_{\mathrm{E}}(1,0)$, (b) $a_{\mathrm{M}}(1,0)$, and (c) $a_{\mathrm{E}}(2,-2) = -a_{\mathrm{E}}(2,2)$.

the multipole, whereas the integer m describes the amount of the z component of angular momentum that is carried per photon. Therefore, the case of $l = 1$ corresponds to a dipole field, $l = 2$ to a quadrupole field, $l = 3$ to an octupole field, and so on.

The expansion in Eqs. (2.17) and (2.18) is a complete [67] and general solution for the scattered field in the region $r > r_0$, where r_0 is the radius of the smallest sphere, centered at the origin, that can enclose the nanoscatterer. To describe the field inside this imaginary sphere, also spherical Hankel functions of the second kind would be required [20]. The coefficients of the multipole expansion depend on the location of the origin of the coordinate system. Thus, in order to minimize the set of multipoles describing a nanoparticle, one should select the origin to lie symmetrically at the center of the particle. Each term of the expansion in Eqs. (2.17) and (2.18) has a unique far-field pattern $\mathbf{F}(\theta, \phi)$. As an example, three far-field patterns, which correspond to an electric dipole, magnetic dipole and an electric quadrupole, are shown in Fig. 2.3.

In order to fully appreciate the expansion in Eqs. (2.17) and (2.18), one can reveal the connection between the scattered field and the actual excitations in the scatterer. As shown in Publication I, the source of the

scattered field can be described with a scattering current density

$$\mathbf{J}_{\mathrm{sca}}(\mathbf{r}) = -\mathrm{i}\omega\big[\varepsilon(\mathbf{r}) - \varepsilon_{\mathrm{h}}\big]\mathbf{E}(\mathbf{r}), \tag{2.19}$$

where $\varepsilon(\mathbf{r})$ is a function giving the permittivity at a certain coordinate $\mathbf{r}$ and ε_{h} is the permittivity of the host medium. Note that the field $\mathbf{E}(\mathbf{r})$ is the total electric field and that the incident plane-wave field satisfies Eqs. (2.1)-(2.4) in the absence of a scatterer, i.e., when $\varepsilon(\mathbf{r}) = \varepsilon_{\mathrm{h}}$. Therefore, Eqs. (2.1)-(2.4) can be written in terms of only the scattered fields by using Eqs. (2.7), (2.8) and (2.19) as

$$\nabla \cdot \mathbf{E}_{\mathrm{sca}}(\mathbf{r}) = -\frac{\mathrm{i}}{\omega\varepsilon_{\mathrm{h}}}\nabla \cdot \mathbf{J}_{\mathrm{sca}}(\mathbf{r}), \tag{2.20}$$

$$\nabla \cdot \mathbf{H}_{\mathrm{sca}}(\mathbf{r}) = 0, \tag{2.21}$$

$$\nabla \times \mathbf{E}_{\mathrm{sca}}(\mathbf{r}) = \mathrm{i}\omega\mu_0\mathbf{H}_{\mathrm{sca}}(\mathbf{r}), \tag{2.22}$$

$$\nabla \times \mathbf{H}_{\mathrm{sca}}(\mathbf{r}) = -\mathrm{i}\omega\varepsilon_{\mathrm{h}}\mathbf{E}_{\mathrm{sca}}(\mathbf{r}) + \mathbf{J}_{\mathrm{sca}}(\mathbf{r}). \tag{2.23}$$

Equations (2.20)-(2.23) are identified as the Maxwell equations describing a current distribution $\mathbf{J}_{\mathrm{sca}}$ that emits an electromagnetic field in a homogeneous space. Therefore, $\mathbf{J}_{\mathrm{sca}}$ can be interpreted as the source of the scattered field. In Publication I, we have expressed the multipole coefficients $a_{\mathrm{E}}(l,m)$ and $a_{\mathrm{M}}(l,m)$ in terms of $\mathbf{J}_{\mathrm{sca}}$. Consequently, if one knows the total electric field inside a scatterer, one can calculate the current density $\mathbf{J}_{\mathrm{sca}}$, the multipole coefficients and, thereby, obtain the scattered field at any point around the scatterer. The advantage of this approach is that it can be applied to a scatterer regardless of the surroundings. Note that the field scattered by a localized particle satisfies Eqs. (2.20)-(2.23) and can, therefore, always be expressed through the multipole expansion. The influence of other scatterers is included self-consistently in $\mathbf{J}_{\mathrm{sca}}$. The total scattered field is obtained by summing the individual contributions of all the scatterers.

It is also possible to obtain the multipole coefficients directly from the scattered field, as shown in Publication I. The coefficients $a_{\mathrm{E}}(l,m)$ can be calculated from the distribution of $\mathbf{r} \cdot \mathbf{E}_{\mathrm{sca}}$ or $\mathbf{r} \times \mathbf{H}_{\mathrm{sca}}$ on any spherical surface of constant r ($r > r_0$). Likewise, the coefficients $a_{\mathrm{M}}(l,m)$ can be calculated from $\mathbf{r} \cdot \mathbf{H}_{\mathrm{sca}}$ or $\mathbf{r} \times \mathbf{E}_{\mathrm{sca}}$ on this surface. There are thereby three different ways to calculate each multipole coefficient, which allows one to double-check the validity of the numerical results. While the approach using the scattered field is simpler than the one using $\mathbf{J}_{\mathrm{sca}}$, it can only be applied to the case of an isolated scatterer. The scattering and extinction

cross sections of a scatterer can be obtained from the multipole coefficients by using equations (20), (22) and (23) of Publication I.

In Publication I, the scattering current density $\mathbf{J}_{\mathrm{sca}}(\mathbf{r})$ excited in a nanoscatterer has been expanded into point current multipoles. The first term in this unconventional expansion is a current dipole that, in fact, coincides with a time-harmonic point electric dipole

$$\mathbf{J}_1(\mathbf{r}) = -\mathrm{i}\omega\mathbf{p}\delta(\mathbf{r}), \tag{2.24}$$

where $\mathbf{p}$ is the electric dipole moment. The next order of current multipoles are current quadrupoles. Each current quadrupole is composed of two current dipoles that oscillate in opposite directions. These dipoles are separated by an infinitesimally small distance either parallel or perpendicular to the directions of the dipoles. The current-quadrupole term in the expansion of $\mathbf{J}_{\mathrm{sca}}(\mathbf{r})$ is written as

$$\mathbf{J}_2(\mathbf{r}) = \mathrm{i}\omega\Big(\overleftrightarrow{\mathbf{Q}} \cdot \nabla\Big)\delta(\mathbf{r}), \tag{2.25}$$

where $\overleftrightarrow{\mathbf{Q}}$ is a dyadic representing the current quadrupole moments. By including higher-order derivatives of the Dirac delta function in the decomposition of $\mathbf{J}_{\mathrm{sca}}(\mathbf{r})$ we obtain all other higher-order current multipoles [PI]. The current multipoles provide a complete orthogonal basis for characterizing electromagnetic excitations in an arbitrary nanoscatterer.

The terms in the expansion of $\mathbf{J}_{\mathrm{sca}}(\mathbf{r})$, which contain the multipole moments, can be mapped onto the expansion coefficients of $\mathbf{E}_{\mathrm{sca}}(\mathbf{r})$, which are the multipole coefficients. The mapping relations up to current octupoles are derived in Publication I. These relations can be used in two ways. First, for a scatterer with a fixed geometry, one can predict the most efficiently excitable current multipoles. The mapping relations then reveal the distribution of the scattered field. Second, for a desired distribution of the scattered field one can calculate the required multipole moments. The geometry of the scatterer can then be designed such that these multipoles will be easy to excite. This is often achieved when the scatterer geometry resembles that of the most significant higher-order current multipole.

One can also map the current multipoles onto time-harmonic versions of the conventional electric and magnetic multipoles that are frequently used in electrostatics and magnetostatics. In this way one can confirm that the three radiation patterns in Fig. 2.3 correspond to an electric dipole, a magnetic dipole and an electric quadrupole. For example, the elements of the electric quadrupole moment $\overleftrightarrow{\mathbf{q}}$ and the magnetic dipole

moment $\mathbf{m}$ are obtained from the current quadrupole $\overleftrightarrow{\mathbf{Q}}$ in Cartesian coordinates as

$$q_{x_u x_v} = \frac{1}{2}(Q_{x_u x_v} + Q_{x_v x_u}), \tag{2.26}$$

$$m_{x_u} = \frac{\mathrm{i}\omega}{2} \sum_{v=1}^{3} \sum_{w=1}^{3} \epsilon_{uvw} Q_{x_v x_w}, \tag{2.27}$$

where ϵ_{uvw} is the Levi-Civita symbol and the Cartesian components of the quantities are labeled with $x_1 \equiv x$, $x_2 \equiv y$ and $x_3 \equiv z$.

It is worthwhile to notice that the multipole expansion can be seen as a generalization of the Mie expansion that is used to analytically solve the problem of scattering by a spherical particle. The Mie expansion can be obtained from the more general Eqs. (2.17) and (2.18) by setting all coefficients with $m \neq \pm 1$ to zero and requiring that $a_{\mathrm{E}}(l,-1) = -a_{\mathrm{E}}(l,1)$ and $a_{\mathrm{M}}(l,-1) = a_{\mathrm{M}}(l,1)$. By comparing the two expansions, one can derive a connection between the Mie expansion coefficients a_l and b_l (from Refs. [13] and [23]) and the multipole coefficients $a_{\mathrm{E}}(l,1)$ and $a_{\mathrm{M}}(l,1)$. This connection is

$$a_{\mathrm{E}}(l,1) = -a_l, \tag{2.28}$$

$$a_{\mathrm{M}}(l,1) = -b_l. \tag{2.29}$$

Thus, the multipole moments in a sphere can be obtained by first calculating the Mie coefficients, a_l and b_l [23], and then using the relations that map the multipole coefficients onto the multipole moments. For more complex scatterers, one must first numerically solve the scattering problem and then calculate the multipole coefficients from either the scattered field or the total field inside the scatterer.

2.4 Two-dimensional nanoparticle arrays

So far, only the case of light scattering by an isolated nanoscatterer has been considered. However, in optical nanomaterials, nanoparticles are arranged in densely packed arrays. In these arrays, each nanoscatterer sees not only the incident light, but also the light scattered by all adjacent nanoscatterers. Consequently, the multipole moments in each nanoparticle are influenced by the inter-particle interaction. In this section, the scattering of a plane wave by a planar array of nanoscatterers is considered. This setup is illustrated in Fig. 2.4.

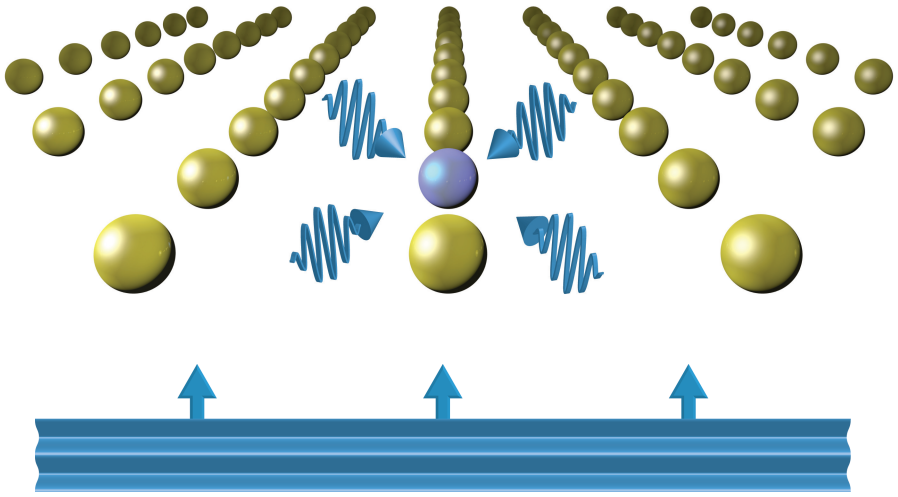

Figure 2.4. A two-dimensional array of nanoscatterers is illuminated by an optical plane wave. In such arrays, a nanoscatterer (blue sphere) interacts not only with the plane wave, but also with the field scattered by adjacent nanoscatterers.

The effect of inter-particle interaction can be illustrated by using a dipolar interaction model [68–71], where small identical scatterers are placed in a periodic square array in the $z = 0$ plane. The scatterers are considered to be small enough to be treatable within the quasi-static approximation. In this case, the scatterers are considered as point dipoles. The array is illuminated by a normally incident plane wave ($\mathbf{k} = k\hat{\mathbf{z}}$ and $\mathbf{E}_0 = E_0\hat{\mathbf{x}}$) that excites an electric dipole moment $p_x = \alpha_{\text{eff}} E_0$ in each of the scatterers. Taking the interactions into account, the effective polarizability α_{eff} of each scatterer can be expressed in SI units as

$$\alpha_{\text{eff}} = \frac{\alpha_0}{1 - \alpha_0 S/(4\pi\varepsilon_{\text{h}})}, \tag{2.30}$$

where α_0 is the polarizability of an isolated particle that can be estimated using quasi-static models [see, e.g., Eqs. (2.15) and (2.16)] or retrieved exactly from the multipole expansion of the scattered field [72]. The array factor S can be calculated from the expression

$$S = \sum_{j \neq i} e^{\mathrm{i}kr_{ij}} \left[\frac{k^2 \sin^2\theta_{ij}}{r_{ij}} + \frac{(1 - \mathrm{i}kr_{ij})(3\cos^2\theta_{ij} - 1)}{r_{ij}^3} \right], \tag{2.31}$$

in which one chooses a certain dipole i and performs the summation over all other dipoles j that are located at $\mathbf{r}_{ij} = r_{ij}(\hat{\mathbf{x}}\cos\theta_{ij} + \hat{\mathbf{y}}\sin\theta_{ij})$. The array factor can also be calculated in the reciprocal space [73]. The inter-particle interaction, provided by S in Eq. (2.30), shifts the resonance wavelength in plasmonic nanoparticles and can produce spectrally sharp lattice resonances [71, 73, 74]. The dipolar interaction model can also be extended to treat uniaxial anisotropic particles at oblique incidence [75] or spherical particles in which electric quadrupole moments are excited [76].

For large nanoparticles in an array, the field scattered by adjacent nanoparticles is no longer constant throughout the volume of the particle. Consequently, numerical techniques are required to treat periodic arrays of such nanoparticles, especially if they are not spherical. Fortunately, the scattering of a plane wave by such an array can be solved by employing periodic boundary conditions, which simplifies the calculations. For example, considering a square array with a period Λ located at $z = 0$, it is sufficient to numerically solve the Maxwell equations only in the region $(x, y) \in ([-\Lambda/2, \Lambda/2], [-\Lambda/2, \Lambda/2])$. The periodic boundary conditions require that the solution at the surface $x = \Lambda/2$ differs from the solution at $x = -\Lambda/2$ only by a factor of $\exp(\mathrm{i}k_x\Lambda)$, where k_x is the x component of the wave vector associated with the incident plane wave. Likewise, the solution at $y = \Lambda/2$ differs from that at $y = -\Lambda/2$ by $\exp(\mathrm{i}k_y\Lambda)$. When the field is calculated, $\mathbf{J}_{\mathrm{sca}}(\mathbf{r})$ can be evaluated inside the scatterers using Eq. (2.19), which can then be used to directly obtain the dipole polarizability α_{eff}, as well as the polarizabilities for all other multipoles (see, e.g., Publications IV and V).

While an individual nanoparticle scatters light in almost all directions, the directions in which light is scattered by a periodic nanoparticle array are considerably restricted. In an array, the multipole fields of adjacent scatterers interfere to form plane waves that propagate only in certain fixed directions. For example, consider a two-dimensional square array of period Λ illuminated by a plane wave with a wave vector $\mathbf{k}$. Assuming the particles to be confined within the region $z \in [-z_0, z_0]$, the scattered electric field outside this region can be expanded into plane waves as [77]

$$\mathbf{E}_{\mathrm{sca}}(x, y, z > +z_0) = \sum_{u=-\infty}^{\infty} \sum_{v=-\infty}^{\infty} \mathbf{E}_{uv} \exp\left[\mathrm{i}(k_{x,\mathrm{sca}}x + k_{y,\mathrm{sca}}y + k_{z,\mathrm{sca}}z)\right], \quad (2.32)$$

$$\mathbf{E}_{\mathrm{sca}}(x, y, z < -z_0) = \sum_{u=-\infty}^{\infty} \sum_{v=-\infty}^{\infty} \mathbf{E}'_{uv} \exp\left[\mathrm{i}(k_{x,\mathrm{sca}}x + k_{y,\mathrm{sca}}y + k_{z,\mathrm{sca}}z)\right], \quad (2.33)$$

where u and v are integers, $\mathbf{E}_{uv}$ and $\mathbf{E}'_{uv}$ are constant vectors, and $k_{x,\mathrm{sca}} = k_x + u2\pi/\Lambda$ and $k_{y,\mathrm{sca}} = k_y + v2\pi/\Lambda$. The periodicity thereby imposes that the components $k_{x,\mathrm{sca}}$ and $k_{y,\mathrm{sca}}$ can differ from the incident wave vector components only by an integer multiple of the reciprocal lattice basis vectors. The z components of the wave vectors satisfy

$$k_{z,\mathrm{sca}} = \begin{cases} +\left[k^2 - (k_{x,\mathrm{sca}}^2 + k_{y,\mathrm{sca}}^2)\right]^{1/2}\mathrm{sign}(z) & \text{for } k^2 > k_{x,\mathrm{sca}}^2 + k_{y,\mathrm{sca}}^2, \\ +\mathrm{i}\left[k_{x,\mathrm{sca}}^2 + k_{y,\mathrm{sca}}^2 - k^2\right]^{1/2}\mathrm{sign}(z) & \text{for } k^2 < k_{x,\mathrm{sca}}^2 + k_{y,\mathrm{sca}}^2. \end{cases} \quad (2.34)$$

The incident plane wave interferes with the forward-scattered plane wave

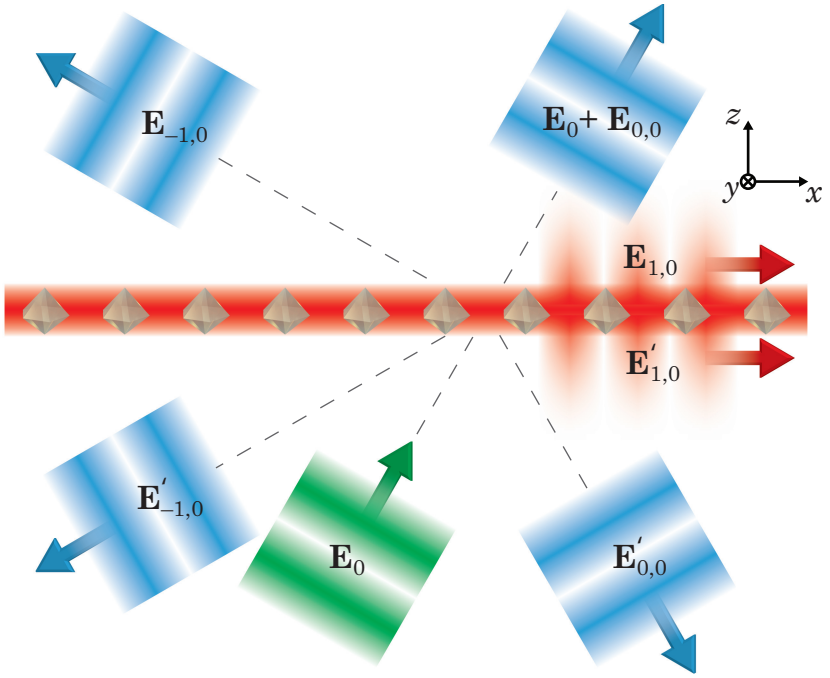

Figure 2.5. Scattering of a plane wave by a two-dimensional square array of nanoscatterers. The incident wave $\mathbf{E}_0$ is split into a transmitted wave ($\mathbf{E}_0 + \mathbf{E}_{0,0}$), a reflected wave ($\mathbf{E}'_{0,0}$), propagating diffracted waves ($\mathbf{E}_{-1,0}$ and $\mathbf{E}'_{-1,0}$) and evanescent waves ($\mathbf{E}_{1,0}$, $\mathbf{E}'_{1,0}$ and higher orders). Propagating and evanescent waves related to the periodicity in y, such as $\mathbf{E}_{0,1}$, also appear (not shown).

$\mathbf{E}_{0,0}$ to form the main transmitted wave. The wave $\mathbf{E}'_{0,0}$ is the main reflected wave. The other waves $\mathbf{E}_{uv}$ and $\mathbf{E}'_{uv}$, which in addition satisfy $k^2 > k_{x,\mathrm{sca}}^2 + k_{y,\mathrm{sca}}^2$, are the propagating diffracted waves. They carry energy away from the array. Thus, the energy of the incident wave is distributed among the transmitted and reflected waves, the propagating diffracted waves and the dissipative excitations in the particles that absorb the field. The waves that satisfy the inequality $k^2 < k_{x,\mathrm{sca}}^2 + k_{y,\mathrm{sca}}^2$ are evanescent, since $k_{z,\mathrm{sca}}$ is imaginary, and do not carry energy away from the array. Instead, they are localized at the array. The appearance of reflected, diffracted and evanescent waves is illustrated in Fig. 2.5.

Equation (2.34) shows that, if $k < \pi/\Lambda$, all diffracted waves are evanescent. In this case, the nanoscatterer array only produces one transmitted and one reflected wave. If only normal-incidence illumination is considered, i.e., $k_x = k_y = 0$, the condition $k < 2\pi/\Lambda$ is enough to ensure that there are no propagating diffraction orders. In the absence of propagating diffraction orders, the array can be characterized by a single transmission and reflection coefficient. The transmission coefficient can be defined as $\tau = 1 + E_{0,0}/E_0$ and the reflection coefficient as $\rho = E'_{0,0}/E_0$, where it is assumed that $\mathbf{E}_{0,0}$, $\mathbf{E}'_{0,0}$ and $\mathbf{E}_0$ are either TE- or TM-polarized. These coefficients naturally depend on both the polarization state and the prop-

agation direction of the incident wave. In Publication II, we model two-dimensional arrays of nanoparticles as infinitely thin sheets with certain τ and ρ. This model turns out to be very efficient and accurate as long as the evanescent waves have a short decay length.

3. Optical nanomaterials

One could suppose that the optical properties of matter are limited by the elements available in the periodic table and their molecular combinations. However, by structuring materials on the nanoscale, optical media with new and sometimes very unusual optical properties can be created. These media belong to the class of optical nanomaterials. In this chapter, we introduce this peculiar type of matter and theoretically describe the phenomenon of light propagation in such nanostructured materials.

3.1 Designed electromagnetic materials

In homogeneous condensed matter, the atoms and molecules are densely packed on a scale much smaller than the wavelength of visible light. As a consequence, light sees the material as a homogeneous medium that can be described by macroscopic material parameters, such as the index of refraction. In analogy, an assembly of nanoscatterers that are packed on a subwavelength scale also appears as a homogeneous material to light. In such nanomaterials, the scatterers behave as "artificial atoms". We call these materials as optical nanomaterials.

By using modern nanotechnology, one can create artificial nanomaterials, in which the scatterers are judiciously designed to provide the material with optical properties unavailable in conventional natural and artificial materials. These designed optical nanomaterials are often coined as optical metamaterials and the nanoscatterers as meta-atoms [78]. The possibility to create materials with derived optical properties has immense potential for unprecedented applications in optics. The most well-known application examples are the invisibility cloak [4, 5, 79–83] and perfect lens [3]. Other interesting effects in metamaterials, which also may lead to real-life applications, are repulsive Casimir force [84, 85], plasmon-

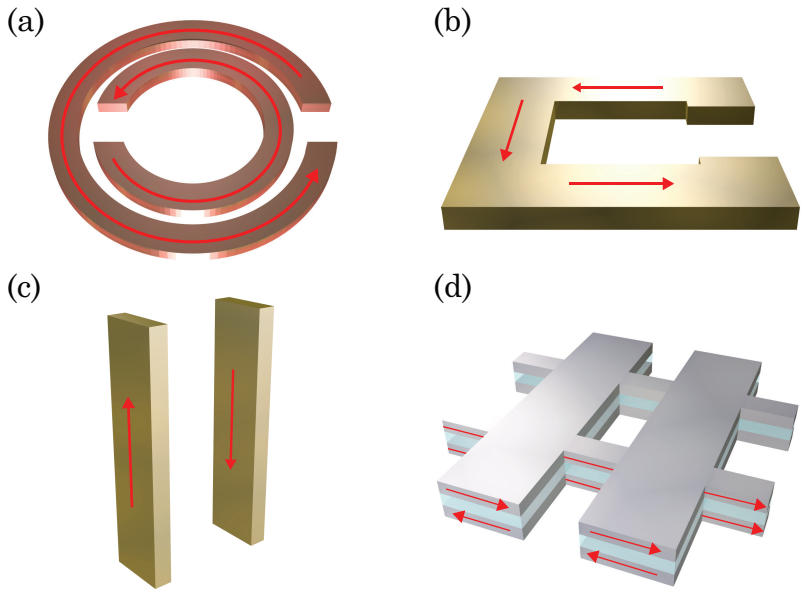

Figure 3.1. Commonly used metallic scatterers in metamaterials: (a) traditional split-ring resonator (SRR), (b) U-shaped SRR, (c) pairs of rods and (d) fishnet structure. The red arrows depict the currents in the structure when the metamaterial exhibits an artificial magnetic response.

induced transparency [86, 87], hyperlens and metalens focusing [88–97], other subwavelength optical effects [98–104], various nanocircuitry phenomena [105–107], self-collimation of light [108] and metamaterial perfect absorbtion [109]. Electromagnetic metamaterials have also served as an inspiration for the creation of other artificial materials, such as acoustic metamaterials [110–113] and quantum metamaterials [114–117].

The metamaterials research was initiated in 1999, when Pendry et al. proposed that an artificial material composed of non-magnetic metal microstructures can respond to microwaves as a magnetic medium with $\mu \neq 1$ [118]. The magnetic response was seen to originate from the excitation of a loop-like current in the structures that were shaped as split-ring resonators (SRR) of the type depicted in Fig. 3.1(a). Soon after, Smith et al. introduced additional thin metal wires alongside the SRRs and showed that the resulting microwave metamaterial would exhibit simultaneously $\mathrm{Re}\{\mu\} < 0$ and $\mathrm{Re}\{\varepsilon\} < 0$ [119]. Such materials can have a negative index of refraction, $\mathrm{Re}\{n\} < 0$. Therefore, they are called negative-index metamaterials (NIM). Simultaneously, the first application of NIMs, the perfect lens that would be able to image objects beyond the diffraction limit was proposed [3]. Then, within the next few years, several NIMs operating in the microwave frequency range were realized [120–123]. Obtaining negative refractive index for visible light, however, was found to be much more challenging [124].

A simple scale-down of the SRRs to nanometer dimensions could not lead to obtaining optical NIMs, since at optical frequencies the electromagnetic response of metals is completely different from that at microwave frequencies [125, 126]. For example, the conductivity decreases and the displacement current inside the metal becomes important [127]. Instead one would have to come up with new designs for the meta-atoms that would provide the required resonant response for obtaining negative refractive index. Artificial magnetism and negative refractive index was subsequently demonstrated in the infrared by using noble metal meta-atoms in the form of U-shaped split-ring resonators [128–131], pairs of rods [132–134] and units of so-called fishnet structures [135–137]. These meta-atoms are depicted in Fig. 3.1. The first NIM design in the visible spectral range (at 780 nm wavelength) was based on the fishnet structure [138]. A major problem for optical NIMs is the large optical absorption in the metal. Typically, any light wave is nearly fully extinguished after propagation through just a few meta-atomic layers of the material. Approaches to tackle this problem involve optimized meta-atom designs [139–144], the use of dielectric meta-atoms [145–147] or optical-gain materials [148].

The prospects of designing optical nanomaterials go much further than just the realization of negative refractive index. For example, optical cloaking would require the use of an anisotropic metamaterial with spatially varying optical properties, without need of a negative refractive index [5]. Even the negative refraction itself can be achieved without resorting to the concept of negative refractive index [149, 150]. Furthermore, propagation of optical beams can be controlled in spatially dispersive nanomaterials, in which the optical properties depend on the propagation direction of the beam's plane-wave components [151]. Also metamaterials with zero [152, 153] and "unnaturally high" refractive indices [154] have been proposed for various optical applications. In Publications I and II we present a general theoretical approach to the characterization of optical meta-atoms and metamaterials, without limiting ourselves to a certain particular property, such as negative refractive index. This approach is then applied to bifacial meta-atoms in Publications III-V.

3.2 Theoretical description

Interaction of light with a nanomaterial is most conveniently described in terms of optical plane waves that are incident onto a slab of the material. Such slabs can be composed by stacking two-dimensional arrays of nanoscatterers in equidistant layers. Usually, these arrays are periodic, which implies that the theory presented in section 2.4 can be applied to each layer of the periodic material. The choice of a periodic arrangement of scatterers is motivated by the ease of fabrication of such structures. They are also most convenient to analyze through numerical calculations. In Publication II, we have presented an interferometric theory that describes the propagation of light through such a nanomaterial slab. In this theory, each two-dimensional array of nanoscatterers is described as an infinitesimally thin sheet with certain plane-wave transmission and reflection coefficients τ and ρ. These coefficients depend on both the polarization and propagation direction of the incident wave. The total transmission and reflection of light by a nanomaterial slab can then be expressed in terms of τ and ρ using a technique that resembles the description of the transmission of a Fabry-Perot interferometer.

In order to describe a nanomaterial slab as a stack of thin sheets, two assumptions must be made. The first assumption is that $k < \pi/\Lambda_{\max}$, which means that all diffracted waves produced by the nanoscatterer layers are evanescent (see section 2.4). Here k is the wave number in the host medium and $\Lambda_{\max}$ is the largest lattice constant of the array. This requirement is necessary for the nanomaterial to be treatable as a homogeneous medium. If the requirement is violated, the nanoscatterers form a photonic crystal [155] rather than a nanomaterial. The second assumption is that the evanescent waves associated with the cut-off diffraction orders do not transfer energy between the nanoscatterer layers. In practice, this requirement can be satisfied by ensuring that the gap d between two nanoscatterers that belong to adjacent arrays is large compared to the decay lengths of the evanescent waves. For the lattice shown in Fig. 3.2(a), the $1/e$ amplitude decay length is [PII]

$$\delta = \left[\left(\frac{2\pi}{\Lambda_x} - k_x \right)^2 - k^2 \right]^{-1/2}. \tag{3.1}$$

In typical nanomaterials with a cubic lattice, the condition $d \gg \delta$ is quite easily satisfied as demonstrated by several examples in Publication II.

Usually, metamaterials are described in terms of effective material parameters that, similarly to the coefficients τ and ρ, also depend on the

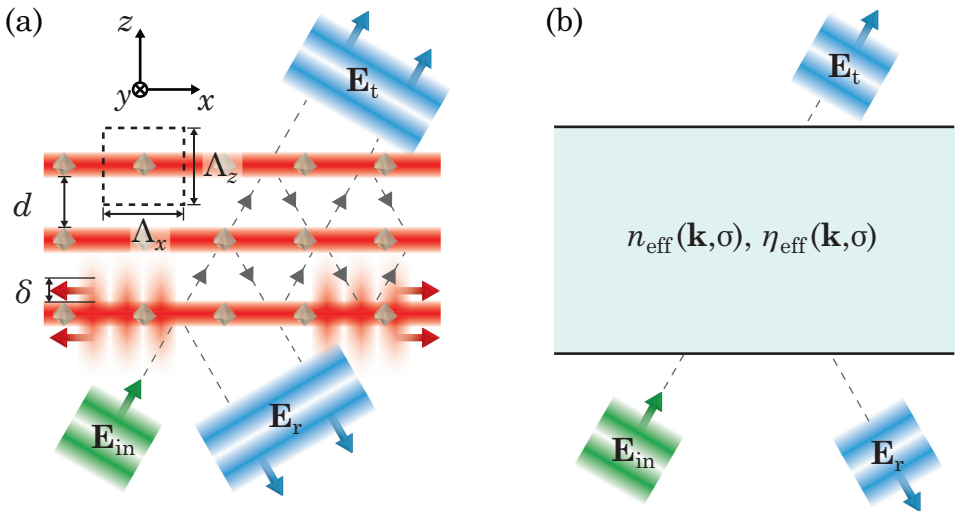

Figure 3.2. (a) Propagation of a plane wave through a stack of two-dimensional nanoscatterer arrays. The evanescent waves extend a distance of δ from each array. Provided that $\delta \ll d$, the interferometric theory can be applied, and the stack can be described as (b) a slab of homogeneous nanomaterial with effective refractive index n_{eff} and wave impedance η_{eff} that are independent of the number of layers composing the slab.

propagation direction and polarization of the wave. For these parameters one can select either the electric permittivity $\varepsilon_{\mathrm{eff}}$ and magnetic permeability μ_{eff} or the refractive index n_{eff} and wave impedance η_{eff}. Their values are usually obtained by using retrieval procedures, in which the transmission and reflection coefficients of a metamaterial slab are fitted to those of an equivalent slab of homogeneous matter [see Fig. 3.2(b)]. An appropriate retrieval procedure was originally introduced only for a wave that is normally incident on a metamaterial slab [156, 157], but was later extended to cover arbitrary incidence angles [12]. In Publication II, we have shown that the interferometric theory can be used to semi-analytically calculate n_{eff}, η_{eff}, $\varepsilon_{\mathrm{eff}}$ and μ_{eff} for homogenizable materials. Provided that the assumptions for the interferometric theory hold, the effective material parameters do not depend on the number of the two-dimensional nanoscatterer arrays in the stack. On the other hand, if these assumptions are violated, evanescent-wave coupling makes the retrieved material parameters depend on the slab thickness [158]. This prevents an unambiguous definition of the effective material parameters, since they do not necessarily converge with an increasing slab thickness [159]. Actually, if the assumptions in question are violated, a negative-index material can become a positive-index material just by changing the slab thickness [160]. In Publication II, we provide simple means to check whether the effective parameters can be introduced for a certain nanomaterial design or not.

The standard retrieval procedures are not general, since they either assume normal incidence illumination [156,157] or that the reflections must be the same from both sides of a metamaterial slab [12]. However, the latter does not hold for optically bifacial nanomaterials, which are composed of noncentrosymmetric nanoscatterers. In such materials, two counterpropagating waves "see" the medium differently. In Publication V, we have used the interferometric theory to derive appropriate effective material parameters for such bifacial nanomaterials. In order to retrieve these parameters, one must first numerically calculate the plane-wave transmission and reflection coefficients for a single two-dimensional array of nanoscatterers. These coefficients depend on the wave vector $\mathbf{k}$ and polarization σ of the plane wave considered, i.e., $\tau = \tau(\mathbf{k}, \sigma)$ and $\rho = \rho(\mathbf{k}, \sigma)$, where $\sigma = \pm 1$ for TE and TM polarization, respectively. The scatterers are assumed to be non-chiral, such that the polarization σ is preserved upon transmission and reflection by each nanoscatterer array. In this case, each such array effectively interacts with only two waves: one propagating with a wave vector $\mathbf{k}$ and the other with a wave vector $\mathbf{k}' = \mathbf{k} - 2\hat{\mathbf{z}}k_z$. This second wave is created by reflections from other arrays in the stack as shown in Fig. 3.2(a). Thus, these two waves have equal k_x and k_y but opposite k_z.

For simplicity, we assume that $\tau(\mathbf{k}, \sigma) = \tau(\mathbf{k}', \sigma)$, which always holds for an array of uniaxial scatterers with the symmetry axis aligned along the z axis. In this case, the effective refractive index n_{eff} and wave impedance η_{eff} can be calculated as [PV]

$$n_{\mathrm{eff}}(\mathbf{k}, \sigma) = \pm \frac{[k_x^2 + k_y^2 + \gamma_z^2]^{1/2}}{k_0}, \tag{3.2}$$

$$\eta_{\mathrm{eff}}(\mathbf{k}, \sigma) = \eta_{\mathrm{h}} \left(\frac{\gamma_z k}{\gamma k_z} \right)^{\sigma} \frac{\rho(\mathbf{k}', \sigma) \exp(\mathrm{i} k_z \Lambda_z) + \{1 - \tau(\mathbf{k}, \sigma) \exp[\mathrm{i}(k_z - \gamma_z)\Lambda_z]\}}{\rho(\mathbf{k}', \sigma) \exp(\mathrm{i} k_z \Lambda_z) - \{1 - \tau(\mathbf{k}, \sigma) \exp[\mathrm{i}(k_z - \gamma_z)\Lambda_z]\}}, \tag{3.3}$$

where $\gamma = n_{\mathrm{eff}} k_0$ is the length of the effective wave vector ($k_0 = \omega\sqrt{\varepsilon_0 \mu_0}$ is the wave number in vacuum). Here, the phase-matching conditions $\gamma_x = k_x$ and $\gamma_y = k_y$ have been used. Equations (3.2) and (3.3) include γ_z, which can be calculated from

$$\gamma_z \Lambda_z = \pm \arccos(a/2) + 2\pi m, \tag{3.4}$$

$$\begin{aligned} a = {} & \exp(\mathrm{i} k_z \Lambda_z)[\tau(\mathbf{k}', \sigma) - \rho(\mathbf{k}, \sigma)\rho(\mathbf{k}', \sigma)\tau(\mathbf{k}, \sigma)^{-1}] \\ & + [\exp(\mathrm{i} k_z \Lambda_z)\tau(\mathbf{k}, \sigma)]^{-1}, \end{aligned} \tag{3.5}$$

with $m \in \mathbb{Z}$. The values for the integer m and the signs in Eqs. (3.2) and (3.4) are chosen as follows: One first calculates τ and ρ for a frequency

that is considerably below the resonance frequencies of the nanoscatterers. At this frequency one has $\gamma_z \approx k_z$, which provides the correct signs and the value for m. Then, one gradually moves towards higher frequencies, while choosing the signs and m such that continuous spectra of γ_z and n_{eff} are obtained. In addition, for lossy nanoscatterers, one can require that $\mathrm{Im}\{\gamma_z\} > 0$ and $\mathrm{Im}\{n_{\mathrm{eff}}\} > 0$.

For bifacial nanomaterials the inequality $\rho(\mathbf{k},\sigma) \neq \rho(\mathbf{k}^{'},\sigma)$ holds and, consequently, by Eq. (3.3) $\eta_{\mathrm{eff}}(\mathbf{k},\sigma) \neq \eta_{\mathrm{eff}}(\mathbf{k}^{'},\sigma)$ is obtained. By reciprocity, it follows that $\rho(\mathbf{k}^{'},\sigma) = \rho(-\mathbf{k},\sigma)$ and therefore also $\eta_{\mathrm{eff}}(\mathbf{k},\sigma) \neq \eta_{\mathrm{eff}}(-\mathbf{k},\sigma) = \eta_{\mathrm{eff}}(\mathbf{k}^{'},\sigma)$. This inequality means that two counter-propagating waves "see" a different wave impedance. Obviously, the reflection of light by a slab of such material depends on the side of illumination. The effective refractive index, however, must be the same for any two counter-propagating waves. This fact is seen from Eq. (3.5). It can be shown to hold also in the case of $\tau(\mathbf{k},\sigma) \neq \tau(\mathbf{k}^{'},\sigma)$ and be considered as a consequence of reciprocity for the waves propagating inside the material. It is noteworthy that the parameters n_{eff} and η_{eff} depend on the propagation direction of the wave, which is rarely the case for natural materials. Because of this, n_{eff} and η_{eff} are often called effective wave parameters [12] and sometimes Bloch material parameters [161].

Using the retrieved n_{eff} and η_{eff}, Fresnel transmission and reflection coefficients can be introduced at a nanomaterial boundary. However, for bifacial nanomaterials the standard Fresnel formulae [162] cannot be applied, since they are obtained by assuming that the material parameters are independent of k. In Publication V, we have derived Fresnel coefficients that are generalized to include also bifacial nanomaterials with uniaxial symmetry. Consider a wave propagating in a nanomaterial with an effective wave vector $(\gamma_x, \gamma_y, \gamma_{z,1})$ and a wave impedance η_1. The wave is incident on an interface with another material, at $z = 0$, giving rise to a reflected and a transmitted wave. The reflected wave has a wave vector $(\gamma_x, \gamma_y, -\gamma_{z,1})$ and impedance $\eta_1^{'}$, whereas the transmitted wave is characterized by $(\gamma_x, \gamma_y, \gamma_{z,2})$ and η_2. The Fresnel transmission and reflection coefficients, τ_{F} and ρ_{F}, are then given by the following expressions [PV]

$$\tau_{\mathrm{F}} = \frac{1/\eta_1 + 1/\eta_1^{'}}{(\gamma_{z,1}/\gamma_1)^{\sigma}/\eta_1^{'} + (\gamma_{z,2}/\gamma_2)^{\sigma}/\eta_2} (\gamma_{z,1}/\gamma_1)^{(\sigma+1)/2} (\gamma_{z,2}/\gamma_2)^{(\sigma-1)/2}, \quad (3.6)$$

$$\rho_{\mathrm{F}} = \frac{(\gamma_{z,1}/\gamma_1)^{\sigma}/\eta_1 - (\gamma_{z,2}/\gamma_2)^{\sigma}/\eta_2}{(\gamma_{z,1}/\gamma_1)^{\sigma}/\eta_1^{'} + (\gamma_{z,2}/\gamma_2)^{\sigma}/\eta_2}, \quad (3.7)$$

where $\sigma = \pm 1$ for the TE and TM polarization, respectively. For spatially non-dispersive materials, i.e., when $\eta_1 = \eta_1^{'}$, these expressions reduce to

the standard Fresnel coefficients. For example, the expressions for the Fresnel coefficients in Ref. [66] are obtained from Eqs. (3.6) and (3.7) by setting $\gamma_j = \sqrt{\mu_j \varepsilon_j} k_0$, $\eta_j = \eta_j^{'} = \sqrt{\mu_j / \varepsilon_j} \eta_0$ and multiplying ρ_{F} with -1 for the TM polarization, since we define the reflected field to have its tangential component in-phase with the tangential component of the incident field for a positive real-valued ρ_{F}.

Together, the effective material parameters in Eqs. (3.2)-(3.5) and the generalized Fresnel coefficients in Eqs. (3.6) and (3.7) can be used to characterize the transmission and reflection by a bifacial nanomaterial slab of an arbitrary thickness. This transmission and reflection can, however, also be described without going through the effort of introducing effective material parameters. Given that the transmission coefficient τ and reflection coefficient ρ of a single two-dimensional nanoparticle array are known, the transmission and reflection coefficients t and r of a stack are obtained as [PII]

$$t = \frac{\tau(\mathbf{k}, \sigma) \exp(\mathrm{i} k_z \Lambda_z)}{G_N - \tau(\mathbf{k}^{'}, \sigma) \exp(\mathrm{i} k_z \Lambda_z) G_{N-1}}, \tag{3.8}$$

$$r = \rho(\mathbf{k}, \sigma) \tau(\mathbf{k}, \sigma)^{-1} G_N t, \tag{3.9}$$

where the G-polynomial is calculated recursively as

$$G_0 = 0, \tag{3.10}$$

$$G_1 = 1, \tag{3.11}$$

$$G_j = a G_{j-1} - \frac{\tau(\mathbf{k}^{'}, \sigma)}{\tau(\mathbf{k}, \sigma)} G_{j-2}, \tag{3.12}$$

with a defined in Eq. (3.5). The results provided by Eqs. (3.8)-(3.12) are identical to those given by applying the generalized Fresnel coefficients to a homogeneous nanomaterial slab. This equality provides a way to verify the calculations. For example, one can numerically calculate t and r for just a two-layer nanomaterial and compare the results to those obtained by using Eqs. (3.8)-(3.12). If they are in agreement, the effective material parameters are physically reasonable and can be introduced to characterize the material.

Using the effective material parameters, one can directly obtain the transmission and reflection at interfaces between the nanomaterial and any homogeneous medium of interest. For example, an air-nanomaterial interface may be of particular interest. As shown in Publication V, the effective material parameters retrieved for a nanomaterial in an infinite host medium of glass give the correct transmission and reflection coefficients for a nanomaterial slab in air.

Recently, optical metamaterials have also been analyzed in terms of Bloch modes. The theory of optical Bloch modes was originally used to describe the propagation of light in photonic crystals [163], and it can be applied to periodic optical metamaterials as well. In the Bloch mode analysis, one considers an infinite three-dimensional periodic array of scatterers and solves for the eigenmodes of the crystal. The solution is thereby forced to satisfy the Bloch periodicity condition in all directions, similarly to what was required for the two-dimensional arrays in Eqs. (2.32) and (2.33). The eigenmodes in the unit cell can be solved by using the Fourier modal method [164]. Once the eigenmodes are solved, one must figure out which of the eigenmodes are excited by plane waves at a boundary of a semi-infinite metamaterial [165]. If the fundamental Bloch mode has the lowest propagation loss in the bulk crystal and if, in addition, it is the only mode that is excited at the metamaterial boundary, then the Fundamental Mode Approximation (FMA) can be applied to the considered plane wave [159]. Only if the FMA holds, can one introduce effective wave parameters that will be independent of the thickness of a metamaterial slab [160]. It is evident that the FMA holds when there is no evanescent-wave coupling between adjacent layers of nanoscatterers in the material. Thus, to design a nanomaterial with thickness-independent effective material parameters, one must either verify that the FMA holds or ensure that the evanescent-wave coupling is negligible. The latter can be verified easily using the interferometric approach of Publication II.

4. Design of nanoparticles and nanomaterials

The optical properties of nanomaterials are determined by the shape, composition and ordering of the nanoparticles that compose the material. Thus, in order to be able to successfully design nanomaterials, both the microscopic and macroscopic aspects of these materials must be considered. The first part of this chapter deals with the microscopic design of individual nanoparticles. It utilizes the multipole theory presented in section 2.3. In the second part, the theory of section 3.2 is harnessed to design the macroscopic optical properties of the nanomaterials. The chapter also unveils the intricate connection between these properties and the multipoles, effectively revealing the connection between the nanoparticles and the nanomaterials.

4.1 Designing the microscopic response

The response of nanoparticles to light, such as their scattering and absorption, fundamentally depend on the particles' geometrical shape. As shown in section 2.2, a deformation of a metal nanosphere into a nanospheroid can significantly change both the strength and the spectral location of its electric dipole resonance, thereby considerably altering its optical response. Furthermore, the geometrical sizes of the nanoparticles used in artificial materials are typically not negligible compared to the wavelength of visible light. Consequently, one must also consider the higher-order multipole excitations in the particles.

As described in section 2.3, the multipole excitations in a nanoscatterer can be revealed by using the methods presented in Publication I. One of them is based on a simple projection of the scattered field onto the terms of the expansion in Eqs. (2.17) and (2.18). In particular, this method has been used to analyze the scattering properties of individual plasmonic

nanoparticles in the form of U-shaped split-ring resonators [166–169], pairs of spheres [166], nanowires [170] and split-ball resonators [171]. The other method, introduced by us in Publication I, retrieves the scattering properties directly from the electric current excitation inside the scatterer and can be applied also to nanoparticle arrays. The multipole analysis is usually performed to reveal the influence of higher-order multipoles on the overall optical response of the particle, since these multipoles can conceptually change the character of the interaction. Higher-order multipoles originate from current excitations of higher complexity than the electric dipole excitation. For example, the second-order multipoles are current quadrupoles, which can be seen as coherent superpositions of conventional magnetic dipoles and electric quadrupoles. In all the results presented in this thesis and the related publications, it was verified that a sufficient number of multipoles were taken into account to accurately describe the scattering properties of the nanoparticles considered.

The importance of the higher-order multipoles can be illustrated by considering the concept of metamaterials with negative refractive index. In these materials, light can resonantly excite both electric and magnetic dipole moments in the unit cells. At frequencies above the central frequencies of these two resonances, the multipoles oscillate essentially out of phase with the incident field. Thus, the meta-atoms can be seen to exhibit effectively negative electric and magnetic dipole polarizabilities [172]. If the resonances are strong enough, this can lead to negative real parts of ε and μ, which can result in a negative refractive index [173]. In many demonstrated negative-index metamaterials, however, the size of the unit cell is still comparable to the wavelength. In this case, also the size and shape of the unit cell influences the effective ε and μ [174]. Another example demonstrating the importance of higher-order multipoles is given in Publication V, where we have shown that in order to suppress optical reflection from a nanomaterial, higher-order multipoles must be excited in the material's unit cells.

The sizes and shapes of currently realizable meta-atoms are typically such that only the two lowest-order current multipoles can be excited. These multipoles are the electric dipole and the current quadrupoles. For example, in the frequently used U-shaped SRR [see Fig. 3.1(b)], two distinct higher-order resonances can be observed [131]. The lower-frequency resonance is a magnetic dipole resonance, whereas the one with higher frequency is mostly of an electric quadrupole nature. However, in meta-

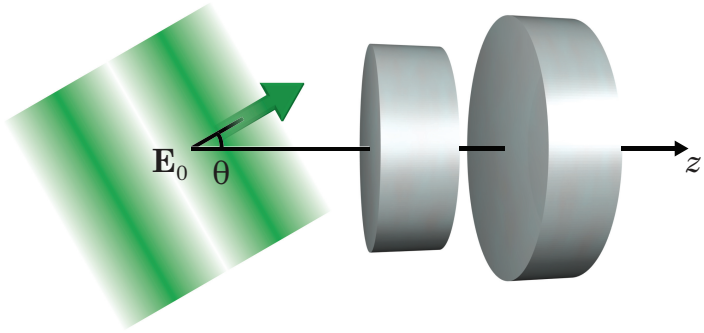

Figure 4.1. Illustration of a nanodimer composed of two axis-aligned silver discs. For a plane-wave excitation, the angle of incidence from the side of the smaller disc is denoted by θ.

atoms made of pairs of metal rods [see Fig. 3.1(c)], the resonant excitation is a pure Cartesian current quadrupole excitation that is composed of a traditional magnetic dipole and electric quadrupole. In Ref. [6], the electric quadrupole was suggested to contribute to the optical properties of metamaterials along with the magnetic dipole. In fact, both the electric quadrupole and the magnetic dipole are second-order current excitations, and neither of them should be neglected when considering the response of a metamaterial to light.

The higher-order multipoles should not be thought of as mere corrections to the electric dipole. In fact, in Publication III, we demonstrate that it is possible to design subwavelength-sized nanoscatterers that, within a certain spectral range, scatter light as pure current quadrupoles. In this range, the electric dipole excitation is suppressed, meaning that the multipole coefficients $a_{\mathrm{E}}(l,m)$ in Eqs. (2.17) and (2.18) are equal to zero for $l = 1$. The nanoscatterer described in Publication III is a disc nanodimer composed of a pair of silver nanodiscs as shown in Fig. 4.1.

The suppression of the electric dipole moment can be explained as follows: One of the discs is chosen to have a smaller diameter, such that its plasmon resonance occurs at a shorter wavelength than the resonance of the larger disc. Qualitatively, each disc can be thought of as an oblate spheroid and, using the results of section 2.2, one can conclude that the larger disc must have a larger resonance wavelength. Thus, at a wavelength between the two resonances of the individual discs, the current in the larger (smaller) disc oscillates out-of-phase (in-phase) with respect to the exciting plane wave. By optimizing the nanodimer geometry, one can obtain equal magnitudes for these two currents, which results in a

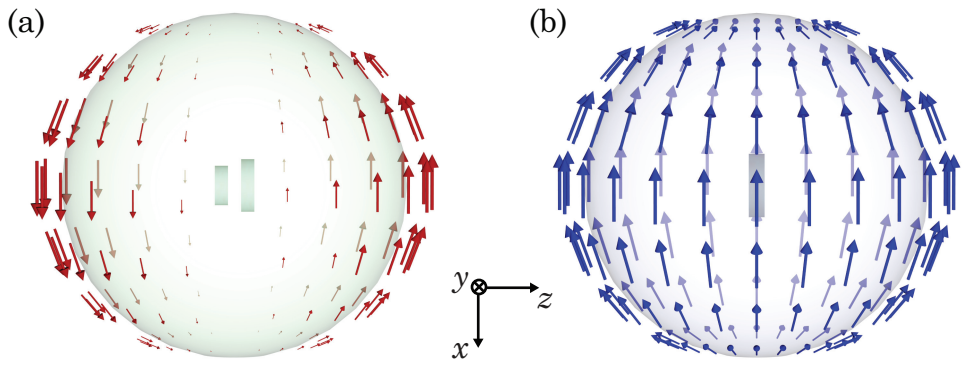

Figure 4.2. The scattered electric field distribution $\mathbf{F}(\theta, \phi)$ [see Eq. (2.9)] of (a) the nanodimer of Fig. 4.1 at the electric-dipole suppression and (b) an electric-dipolar scatterer in the form of a disc.

zero net electric dipole moment. In our optimized design, both discs have a thickness of 10 nm and they are separated by a gap of 10 nm. The diameters of the smaller and larger discs are 30 nm and 40 nm, respectively. The surrounding host medium is assumed to have a refractive index of 1.5. When the nanodimer is illuminated by an optical plane wave from the smaller-disc side (at $\theta = 0$), the dipole suppression is observed at a vacuum wavelength of $\lambda_0 \approx 592$ nm.

The field scattered by the nanodimer is a superposition of the electric quadrupole field [$a_{\mathrm{E}}(l, m)$ with $l = 2$] and the magnetic dipole field [$a_{\mathrm{M}}(l, m)$ with $l = 1$]. The subwavelength size of the nanodimer ensures that the multipole coefficients are not sensitive to the exact location of the origin of the coordinate system. The fields scattered by the discs in the directions perpendicular to the dimer axis destructively interfere. As a consequence, the scattered radiation is highly directional, as depicted in Fig. 4.2(a). For comparison, Fig. 4.2(b) illustrates the far-field of an electric dipole, a typical field pattern for subwavelength-sized scatterers of simple geometrical shapes.

Since the multipole coefficients can be retrieved from the electric field distribution inside the particle [PI], the multipole decomposition of the scattered field can be performed regardless of the surroundings. This possibility is often overlooked. For example, in Ref. [168], it is assumed that the multipole approach cannot be applied to scatterers in close proximity of other scatterers or interfaces. However, the electric dipole moments of the individual discs composing the nanodimer were correctly obtained from the field distributions inside the individual particles. The spectra of these dipole moments are shown in figure 3 of Publication III.

In Publication IV, we present an analytical model for the multipole

polarizabilities of a single nanodimer. The scattering characteristics of the nanodimer are anisotropic and spatially dispersive, i.e., they depend on the polarization and the angle of incidence θ of the incident wave. Apart from truly spherical nanoparticles, nanoscatterers in practice always exhibit some degree of spatial dispersion at visible frequencies. In the widely used U-shaped SRRs, for example, spatial dispersion is significant [11]. As a consequence, the polarizabilities of these particles must also depend on the angle of incidence.

For optical characterization of the nanodimer, the current multipoles form a much more convenient basis than the conventional electric and magnetic multipoles. The electric dipole moment $\mathbf{p}$ and current quadrupole moment $\overleftrightarrow{\mathbf{Q}}$ that a plane wave excites in the nanodimer can be expressed as

$$\mathbf{p}(\theta) = \overleftrightarrow{\alpha}(\theta) \cdot \mathbf{E}_0, \tag{4.1}$$

$$\overleftrightarrow{\mathbf{Q}}(\theta) = \overleftrightarrow{\beta}(\theta) \cdot \mathbf{E}_0, \tag{4.2}$$

where $\overleftrightarrow{\alpha}$ and $\overleftrightarrow{\beta}$ are the spatially dispersive multipole polarizability tensors. In Publication IV, we have shown both numerically and by using a simple analytical model that the elements of the polarizability tensors can quite accurately be expressed as

$$\alpha_{xx} = \alpha_{yy} = a_1 + \frac{1-\cos\theta}{2}\tilde{a}_1, \tag{4.3}$$

$$\alpha_{zz} = a_2, \tag{4.4}$$

$$\beta_{xzx} = \beta_{yzy} = b_1 + \frac{1-\cos\theta}{2}\tilde{b}_1, \tag{4.5}$$

$$\beta_{zxx} = \beta_{zyy} = b_2 + \frac{1-\cos\theta}{2}\tilde{b}_2, \tag{4.6}$$

where the coefficients a_1, $\tilde{a}_1$, a_2, b_1, $\tilde{b}_1$, b_2, $\tilde{b}_2$ depend on the excitation frequency, but are independent of the propagation direction.

Equations (4.1)-(4.6) provide a phenomenological model for the interaction of light with nanodimers. Similar models can be introduced also for other meta-atom designs. For example, in Ref. [175], spatially dispersive polarizabilities are obtained for a U-shaped SRR. The use of polarizabilities is insightful when characterizing not only individual nanoscatterers, but also nanoparticles inside nanomaterials. For example, the nanoparticle interaction model presented in section 2.4 could be improved by including also quadrupole excitations in the particles. Thereby, Eqs. (4.1)-(4.6) could be incorporated into the description of two-dimensional arrays of nanodimers. A three-dimensional nanomaterial could subsequently be

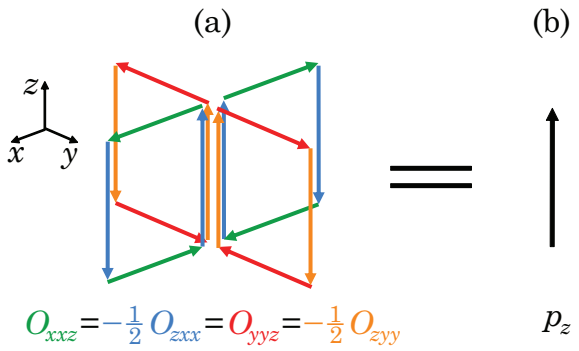

Figure 4.3. Electric current distributions in (a) a toroidal dipole and (b) an electric dipole. In terms of current multipoles, the toroidal dipole is a current octupole. Each arrow represents a time-harmonic current element. The fields created by the toroidal and electric dipoles are indistinguishable from each other. Adapted from Publication I, where the distribution in (a) is treated as a current octupole.

described in terms of the two-dimensional arrays, as will be shown in the next section.

The expansion of a current excitation into conventional electric and magnetic multipoles is incomplete, because in the third and higher order terms of the expansion the so-called toroidal multipoles [176] are neglected. In contrast, the expansion into electric current multipoles introduced in Publication I is complete and inherently includes all electric, magnetic and toroidal multipoles. In particular, the third-order current excitations (current octupoles) include electric octupoles, magnetic quadrupoles and toroidal dipoles. The toroidal multipole moments generate electromagnetic fields that interfere with the fields of conventional electric and magnetic multipoles. As an example, a point toroidal dipole oriented along the z direction is shown in Fig. 4.3(a). The corresponding current distribution

$$\mathbf{J}_{\mathrm{tor}}(\mathbf{r}) = -2\mathrm{i}\omega O_{xxz}\left(\hat{\mathbf{x}}\frac{\mathrm{d}}{\mathrm{d}x}\frac{\mathrm{d}}{\mathrm{d}z} + \hat{\mathbf{y}}\frac{\mathrm{d}}{\mathrm{d}y}\frac{\mathrm{d}}{\mathrm{d}z} - \hat{\mathbf{z}}\frac{\mathrm{d}^2}{\mathrm{d}x^2} - \hat{\mathbf{z}}\frac{\mathrm{d}^2}{\mathrm{d}y^2}\right)\delta(\mathbf{r}) \tag{4.7}$$

contains four non-zero current octupole moments that satisfy the conditions $O_{xxz} = O_{yyz} = -\frac{1}{2}O_{zxx} = -\frac{1}{2}O_{zyy}$. The current distribution of a z-oriented dipole [see Fig. 4.3(b)] is

$$\mathbf{J}_{\mathrm{dip}}(\mathbf{r}) = -\mathrm{i}\omega p_z \hat{\mathbf{z}}\delta(\mathbf{r}). \tag{4.8}$$

This distribution is orthogonal to the distribution in Eq. (4.7). As shown in Publication I, the currents in Eqs. (4.7) and (4.8) create exactly the same dipole fields [see Fig. 4.2(b)] when $p_z = 2O_{xxz}k^2$.

In a nanodimer that consists of two plasmonic elements, one can efficiently excite the second-order multipoles. In analogy, nanoscatterers allowing the third-order multipole excitations can be constructed out of four

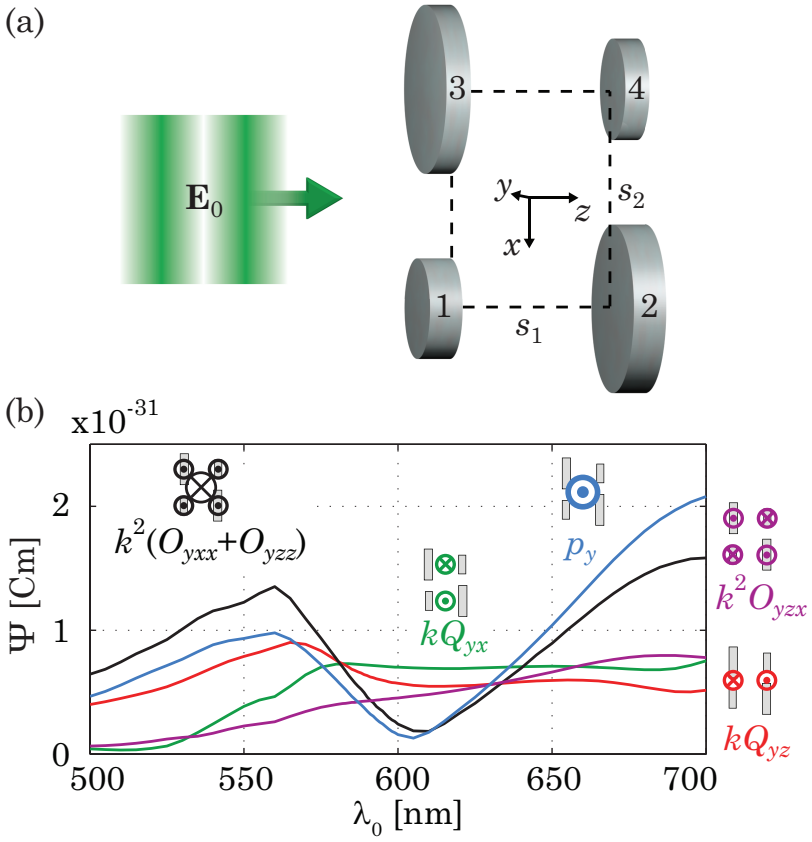

Figure 4.4. (a) Illustration of a nanoquadrimer composed of four axis-aligned silver discs. The radii and thicknesses of the four discs (labeled in the figure) are $[R_1, R_2, R_3, R_4] = [30, 50, 50, 25]$ and $[h_1, h_2, h_3, h_4] = [20, 20, 15, 15]$ in nm. The surface-to-surface separation in the z direction and the center-to-center separation in the x direction are $s_1 = 100$ nm and $s_2 = 130$ nm, respectively. (b) The absolute values of the dominant normalized multipole moments Ψ for the case of a y-polarized incident wave propagating in the z direction with an electric field amplitude of 1 V/m. The current quadrupole moments are multiplied with the wave number in the host medium k (refractive index $n = 1.5$). The current octupole moments are multiplied with k^2.

plasmonic elements. Such a nanoquadrimer is depicted in Fig. 4.4(a). Let us assume that a y-polarized plane wave propagating in a host medium of refractive index 1.5 is incident onto this nanoquadrimer. Using the numerically obtained scattered field, we calculate the coefficients of the multipole expansion. Then, using the theory in Publication I, we map these coefficients onto the current multipole moments. In general, 18 orthogonal current octupoles exist (9 electric octupoles, 6 magnetic quadrupoles and 3 toroidal dipoles), but only 12 coefficients appear in the multipole expansion. Therefore, in order to unambiguously determine the multipole moments, one must use the geometry of the scatterer and eliminate weak or symmetry-forbidden excitations. In the quadrimer, the incident wave efficiently excites only the current octupoles O_{yzx}, O_{yxx}, O_{yzz}, O_{xxy} and O_{xyz}. Consequently, we solve for these moments in addition to the current

dipole and quadrupole moments. The excitations O_{xxy} and O_{xyz} turn out to be rather weak and the excitations O_{yxx} and O_{yzz} are observed to be essentially in phase across the whole visible spectral range. Among the current dipoles and quadrupoles, only p_y, Q_{yz} and Q_{yx} are found to have considerable values.

In Fig. 4.4(b) the absolute values of the most significant multipole moments are shown. In order for the multipoles of different orders to have comparable magnitudes, the quadrupole moment is multiplied with k and the octupole moment with k^2. This normalization is based on the fact that the electric far-field radiated by a current multipole of order l scales with k^{l+1}. The electric current distributions of the multipole excitations are illustrated in the insets of Fig. 4.4(b). From the spectra we see that the excitation $O_{yxx} + O_{yzz}$, in which $O_{yxx} = O_{yzz}$, appears along-side with the dipole moment p_y. The excitation $O_{yxx} + O_{yzz}$ is explained by the fact that the four current elements are displaced from the center of the nanoquadrimer by a distance that is a considerable fraction of the wavelength. The superposition of p_y and $O_{yxx} + O_{yzz}$ results in four current elements that oscillate in phase. At wavelengths around $\lambda_0 = 605$ nm, this in-phase excitation is suppressed and the octupole O_{yzx} becomes more significant. In an ideal O_{yzx} excitation, the currents in discs 1 and 4 oscillate out of phase with the currents in discs 2 and 3, and all four currents have the same amplitude. However, the realistic currents are not so well matched in amplitudes and phases and, therefore, current quadrupole moments Q_{yz} and Q_{yx} appear in addition to the octupoles. The example of the nanoquadrimer demonstrates that a rigorous description of the field scattered by a complex meta-molecule in terms of the elementary current excitations is possible.

4.2 Designing the macroscopic response

The design of functional optical nanomaterials can be greatly simplified by using the analysis of the current multipole excitations in the material's unit cells. These multipoles reveal the influence of the meta-atomic geometry on the macroscopic optical properties of the materials. In the light-nanomaterial interaction picture, the densely packed nanoparticles interact with both the incident field and with the fields scattered by the adjacent nanoparticles. Consequently, the multipole polarizabilities of the scatterers are modified by the inter-particle interaction. Crystalline nano-

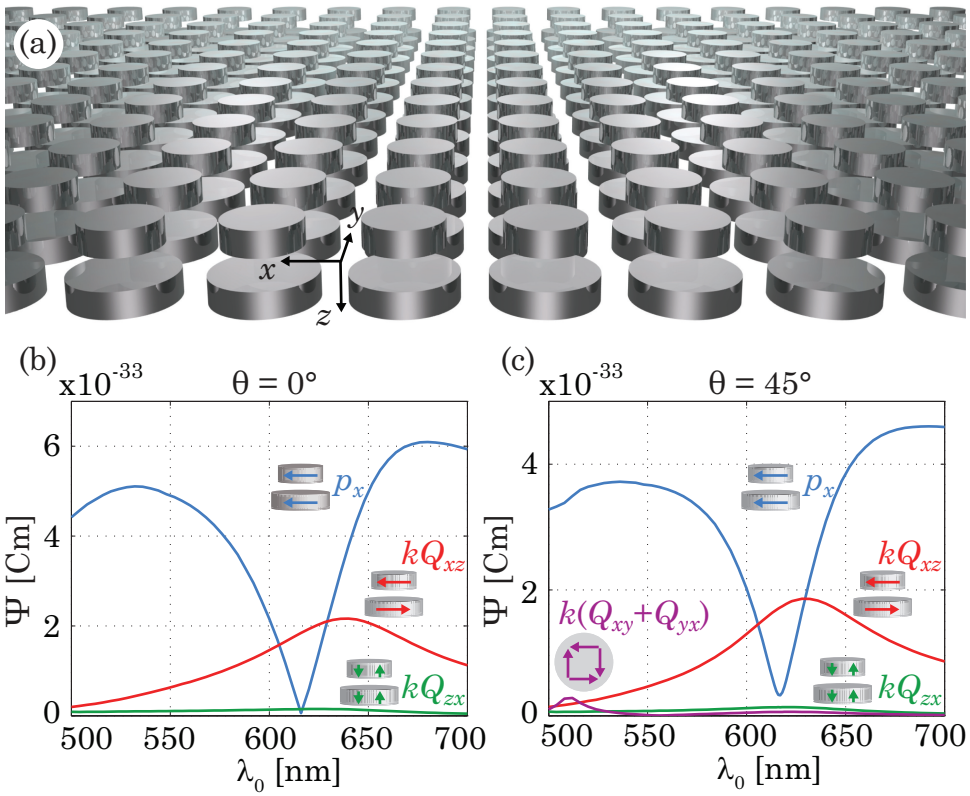

Figure 4.5. (a) Illustration of a two-dimensional array composed of the silver nanodimers of Fig. 4.1. The absolute values of the dominant normalized multipole moments Ψ are shown for (b) normal incidence and (c) a TE-polarized plane-wave incident at an angle of $\theta = 45°$. The current quadrupole moments are multiplied with k (refractive index $n = 1.5$). The incident wave has an electric field amplitude of 1 V/m.

materials can be treated as stacks of two-dimensional periodic arrays, as described in section 3.2. Using the theory reported in Publication I, one can extract the multipole excitations in each two-dimensional array and then use the results to characterize the whole three-dimensional nanomaterial.

Let us consider a two-dimensional array of the disc nanodimers treated in the previous section (see Fig. 4.1). In this array, the dimers are arranged in a square lattice of period $\Lambda = 50$ nm in the $z = 0$ plane. This configuration is shown in Fig. 4.5(a) and it is the same as that presented in Publication III. The absolute values of the dominant normalized multipole moments excited in the dimers are shown in Fig. 4.5(b). Here the array is illuminated by a normally incident plane wave propagating in the positive z direction. The electric dipole moment p_x is suppressed at a wavelength of $\lambda_0 \approx 618$ nm. The suppression wavelength is red-shifted with respect to that of the individual nanodimer, because of the inter-particle interaction. At $\lambda_0 \approx 618$ nm, the Q_{xz} current quadrupole is the dominant excitation. The orthogonal quadrupole Q_{zx} is much weaker. In Fig. 4.5(c)

the multipole moments are shown for a TE-polarized plane wave incident at an angle of $\theta = 45°$. In this case, the strength of the dipole moment is still suppressed below that of the current quadrupole moment, but it is no longer completely cancelled. Furthermore, at $\lambda_0 \approx 510$ nm, an electric quadrupole resonance with $Q_{xy} = Q_{yx}$ appears. The electric current distributions of the significant multipole excitations are illustrated in the insets of Figs. 4.5(b) and (c).

The incident wave will be partially transmitted and reflected by the array. The resulting waves are fully determined by the fields that the multipoles together radiate. For example, in Publication V, we have expressed the normal-incidence transmission and reflection coefficients, τ and ρ, of nanoparticle arrays in terms of the excited current multipole moments. For the considered x-polarized incident wave, only the current multipoles p_x and Q_{xz} were needed to be considered, since p_y and Q_{yz} would create a y-polarized plane wave, which would be impossible for scatterers preserving the light polarization state. The remaining 8 elements of $\mathbf{p}$ and $\overleftrightarrow{\mathbf{Q}}$ are such that they do not radiate in the $\pm\hat{\mathbf{z}}$ directions.

In the following, the formalism in Publication V is extended to oblique incidence. For simplicity, we only take into account the contribution of p_x and Q_{xz}, which are the dominant excitations in the nanodimer for TE-polarized incident light [PIV]. The field scattered by meta-atoms in a periodic two-dimensional square lattice that is located in the $z = 0$ plane can be written as

$$\mathbf{E}_{\mathrm{lat}}(\mathbf{r}) = \sum_{u=-\infty}^{\infty} \sum_{v=-\infty}^{\infty} \mathbf{E}(\mathbf{r} - u\Lambda\hat{\mathbf{x}} - v\Lambda\hat{\mathbf{y}}) \exp[\mathrm{i}(k_x x + k_y y)], \tag{4.9}$$

where $\mathbf{E}$ is the field created by an individual particle, i.e., it satisfies the multipole expansion in Eqs. (2.17) and (2.18). The exponential term provides the phase-matching of the particle excitations with the incident plane wave. Following the mathematical procedure of Ref. [77], $\mathbf{E}_{\mathrm{lat}}(\mathbf{r})$ can be expressed in terms of the angular spectrum [66] of $\mathbf{E}(\mathbf{r})$ as

$$\begin{aligned}\mathbf{E}_{\mathrm{lat}}(\mathbf{r}) =& \Big(\frac{2\pi}{\Lambda}\Big)^2 \sum_{u=-\infty}^{\infty} \sum_{v=-\infty}^{\infty} \tilde{\mathbf{E}}_{\pm}(k_x + u\frac{2\pi}{\Lambda}, k_y + v\frac{2\pi}{\Lambda}) \\ & \exp\left[\mathrm{i}(k_x + u\frac{2\pi}{\Lambda})x + \mathrm{i}(k_y + v\frac{2\pi}{\Lambda})y + \mathrm{i}k_{z,\mathrm{sca}}z\right],\end{aligned} \tag{4.10}$$

where $\pm$ denotes the angular spectra at $z > 0$ and $z < 0$, respectively. The definition of $k_{z,\mathrm{sca}}$ is given in Eq. (2.34). Only the term with $(u, v) = (0, 0)$ contributes to the transmitted and reflected waves when $k < \pi/\Lambda$. All other combinations of u and v correspond to diffracted waves (see section 2.4) that are evanescent for any two-dimensional array composing a

homogenizable optical nanomaterial. Thus, we can immediately express the reflection and transmission coefficients for a given polarization state of the incident field $\mathbf{E}_0$ as

$$\rho = \Big(\frac{2\pi}{\Lambda}\Big)^2 \frac{\tilde{\mathbf{E}}_-(k_x,k_y)\cdot(\mathbf{E}_0 - 2\mathbf{E}_0\cdot\hat{\mathbf{z}}\hat{\mathbf{z}})^*}{|E_0|^2}, \tag{4.11}$$

$$\tau = 1 + \Big(\frac{2\pi}{\Lambda}\Big)^2 \frac{\tilde{\mathbf{E}}_+(k_x,k_y)\cdot\mathbf{E}_0^*}{|E_0|^2}, \tag{4.12}$$

where it is assumed that the exciting plane wave is incident on the array from the $z<0$ half-space. These coefficients are calculated with respect to the plane $z=0$. Equations (4.11) and (4.12) relate the angular spectrum of the field scattered by an individual particle to τ and ρ.

The scattering by an individual particle can be characterized by using the multipole expansion. For each multipole, we can calculate $\tilde{\mathbf{E}}_\pm(k_x,k_y)$ and thereby obtain τ and ρ. For an electric dipole, the vector potential in the Lorenz gauge is [PI]

$$\mathbf{A}_1(\mathbf{r}) = -\frac{\mathrm{i}}{\omega}\frac{k^2\mathbf{p}}{4\pi\varepsilon_\mathrm{h}}\frac{\exp(\mathrm{i}kr)}{r}. \tag{4.13}$$

Using the Weyl representation of a spherical wave [177], we can write

$$\mathbf{A}_1(\mathbf{r}) = \frac{1}{\omega}\frac{k^2\mathbf{p}}{8\pi^2\varepsilon_\mathrm{h}}\int_{-\infty}^{\infty}\int_{-\infty}^{\infty}\frac{\exp(\mathrm{i}\mathbf{K}\cdot\mathbf{r})}{|K_z|}dK_x dK_y, \tag{4.14}$$

where

$$K_z = \begin{cases} +\big[k^2-(K_x^2+K_y^2)\big]^{1/2}\mathrm{sign}(z) & \text{for } k^2 > K_x^2+K_y^2, \\ +\mathrm{i}\big[K_x^2+K_y^2-k^2\big]^{1/2}\mathrm{sign}(z) & \text{for } k^2 < K_x^2+K_y^2. \end{cases} \tag{4.15}$$

The electric field follows from the vector potential as [PI]

$$\mathbf{E}(\mathbf{r}) = \mathrm{i}\omega\Big\{\mathbf{A}(\mathbf{r}) + \frac{1}{k^2}\nabla\big[\nabla\cdot\mathbf{A}(\mathbf{r})\big]\Big\}. \tag{4.16}$$

By inserting Eq. (4.14) into (4.16), we obtain the angular spectrum decomposition of $\mathbf{E}$. If the dipole is x-oriented, the angular spectrum is

$$\tilde{\mathbf{E}}_1(K_x,K_y) = \frac{\mathrm{i}p_x}{8\pi^2\varepsilon_\mathrm{h}|K_z|}\big[(k^2-K_x^2)\hat{\mathbf{x}} - K_xK_y\hat{\mathbf{y}} - K_xK_z\hat{\mathbf{z}}\big]. \tag{4.17}$$

In an analogous manner, we calculate the field originating from the current quadrupole Q_{xz}. In this case, the vector potential is [PI]

$$\mathbf{A}_2(\mathbf{r}) = \frac{\mathrm{i}}{\omega}\frac{k^2Q_{xz}}{4\pi\varepsilon_\mathrm{h}}\hat{\mathbf{x}}\frac{\mathrm{d}}{\mathrm{d}z}\frac{\exp(\mathrm{i}kr)}{r}. \tag{4.18}$$

Following the same procedure as for the electric dipole, we obtain the angular spectrum of the field created by the current quadrupole Q_{xz} to be

$$\tilde{\mathbf{E}}_2(K_x,K_y) = \frac{Q_{xz}K_z}{8\pi^2\varepsilon_\mathrm{h}|K_z|}\big[(k^2-K_x^2)\hat{\mathbf{x}} - K_xK_y\hat{\mathbf{y}} - K_xK_z\hat{\mathbf{z}}\big]. \tag{4.19}$$

The transmission and reflection coefficients are obtained by evaluating the angular spectra at $K_x = k_x$, $K_y = k_y$ and, consequently, $K_z = \pm k_z$ in the $z > 0$ and $z < 0$ half-spaces, respectively.

For the TE polarization, one can for example consider the case of $\mathbf{k} = \hat{\mathbf{y}}k_y + \hat{\mathbf{z}}k_z$ and $\mathbf{E}_0 = E_0\hat{\mathbf{x}}$. Assuming that the wave excites both p_x and Q_{xz} simultaneously, we use Eqs. (4.11) and (4.12) and obtain

$$\rho_{\mathrm{TE}} = \frac{\mathrm{i}(p_x + \mathrm{i}k_z Q_{xz})}{2\varepsilon_{\mathrm{h}}\Lambda^2 E_0}\frac{k^2}{k_z}, \tag{4.20}$$

$$\tau_{\mathrm{TE}} = \frac{\mathrm{i}(p_x - \mathrm{i}k_z Q_{xz})}{2\varepsilon_{\mathrm{h}}\Lambda^2 E_0}\frac{k^2}{k_z} + 1. \tag{4.21}$$

For the TM polarization, we can choose, e.g., $\mathbf{k} = \hat{\mathbf{x}}k_x + \hat{\mathbf{z}}k_z$ and $\mathbf{E}_0 = E_0(\hat{\mathbf{x}}k_z/k - \hat{\mathbf{z}}k_x/k)$. In this case the coefficients are

$$\rho_{\mathrm{TM}} = \frac{\mathrm{i}(p_x + \mathrm{i}k_z Q_{xz})}{2\varepsilon_{\mathrm{h}}\Lambda^2 E_0}k, \tag{4.22}$$

$$\tau_{\mathrm{TM}} = \frac{\mathrm{i}(p_x - \mathrm{i}k_z Q_{xz})}{2\varepsilon_{\mathrm{h}}\Lambda^2 E_0}k + 1. \tag{4.23}$$

It can be noted from Eqs. (4.20)-(4.23) that, for a dipolar array, the coefficients are always connected as $\tau = 1 + \rho$. On the other hand, when the current quadrupoles are present, τ and ρ do not have a one-to-one correspondence. For example, the reflection coefficient can become equal to zero or dependent on the direction of illumination [PV]. For normal-incidence illumination ($\mathbf{k} = k\hat{\mathbf{z}}$), Eqs. (4.20)-(4.23) reduce to the expressions given in Publication V. These expressions are

$$\rho_0 = \frac{\mathrm{i}k}{2\varepsilon_{\mathrm{h}}\Lambda^2 E_0}(p_x + \mathrm{i}kQ_{xz}), \tag{4.24}$$

$$\tau_0 = \frac{\mathrm{i}k}{2\varepsilon_{\mathrm{h}}\Lambda^2 E_0}(p_x - \mathrm{i}kQ_{xz}) + 1. \tag{4.25}$$

The multipole moments calculated for the nanodimer array of Fig. 4.5 can be inserted into Eqs. (4.20)-(4.23) to obtain τ and ρ. The results can then be compared to the results of direct numerical calculations, in which the amplitudes and phases of the transmitted and reflected waves are evaluated far away from the array. This comparison is shown in Fig. 4.6 for both TE- and TM-polarized waves incident at $\theta = 45°$. For the TE polarization, the agreement between the two calculations is essentially perfect, as shown in Fig. 4.6(a). It is interesting that a small discrepancy at $\lambda_0 = 510$ nm is caused by the neglect of the weak electric quadrupole excitation with $Q_{xy} = Q_{yx}$, shown in Fig. 4.5(c). For the TM polarization, the dipole moment p_z that is omitted in Eqs. (4.22) and (4.23) is also excited. Consequently, the calculated coefficients are not exact, which is seen in Fig. 4.6(b). The individual complex-valued contributions of p_x and Q_{xz}

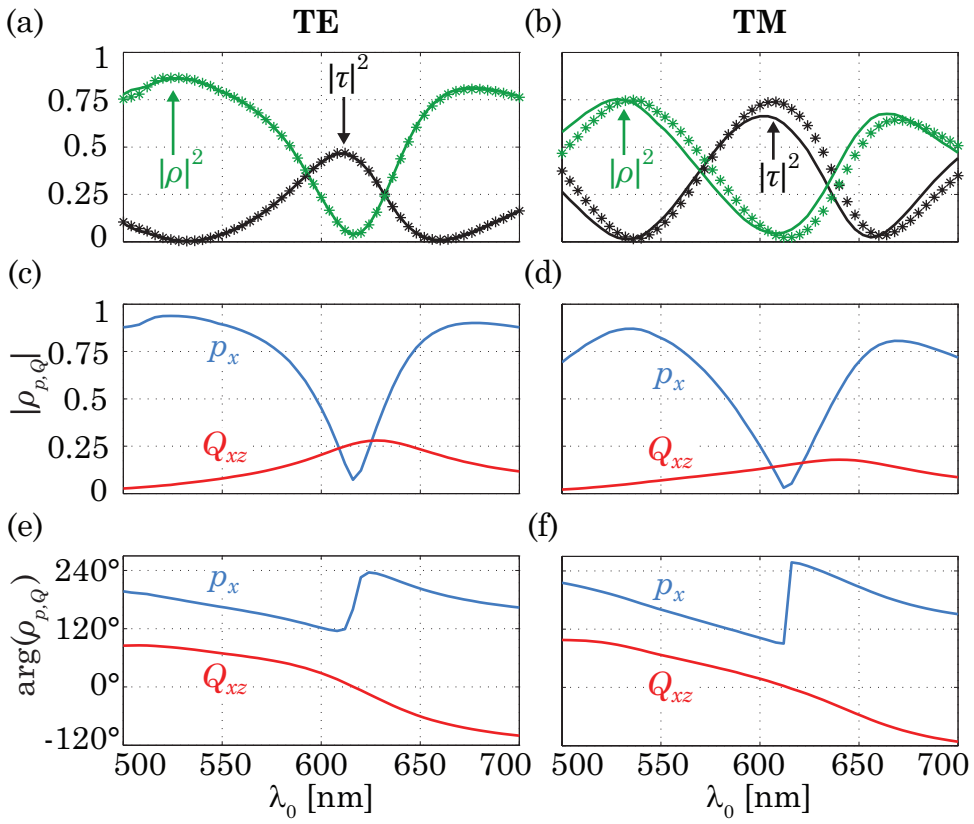

Figure 4.6. Intensity transmission and reflection coefficients of the nanodimer array in Fig. 4.5 for (a) TE-polarized and (b) TM-polarized waves that are incident at $\theta = 45°$. The solid lines in (a) and (b) are obtained directly from the computed far-field, whereas the stars are calculated from the multipole moments in the unit cells by using Eqs. (4.20)-(4.23). The individual complex-valued contributions of p_x and Q_{xz} to ρ are also shown separately (c,e) for TE polarization and (d,f) for TM polarization.

to ρ in Eqs. (4.20) and (4.22) are shown in Figs. 4.6(c)-(f). The phases of the contributions of p_x rapidly change in the spectral range of the dipole suppression. This is explained by the fact that the net dipole moment reverses its direction when crossing the minimum at $\lambda_0 \approx 618$ nm. For $\lambda_0 \gtrsim 618$ nm, the field produced by the larger disc, which oscillates out of phase with the incident field, dominates. On the other hand, for $\lambda_0 \lesssim 618$ nm, the in-phase oscillating field radiated by the smaller disc dominates. If necessary, the contribution of any higher-order multipole to τ and ρ can be obtained by applying a similar derivation procedure as was done for p_x and Q_{xz}.

After choosing a desired two-dimensional array of nanoscatterers, one can proceed to stack such arrays into a three-dimensional crystal that can be treated using the theory of section 3.2. It only remains to choose the longitudinal period Λ_z. This choice naturally influences the spatially dispersive effective material parameters of the resulting nanomaterial. If Λ_z is chosen to be too small relative to Λ_x and Λ_y, evanescent-wave cou-

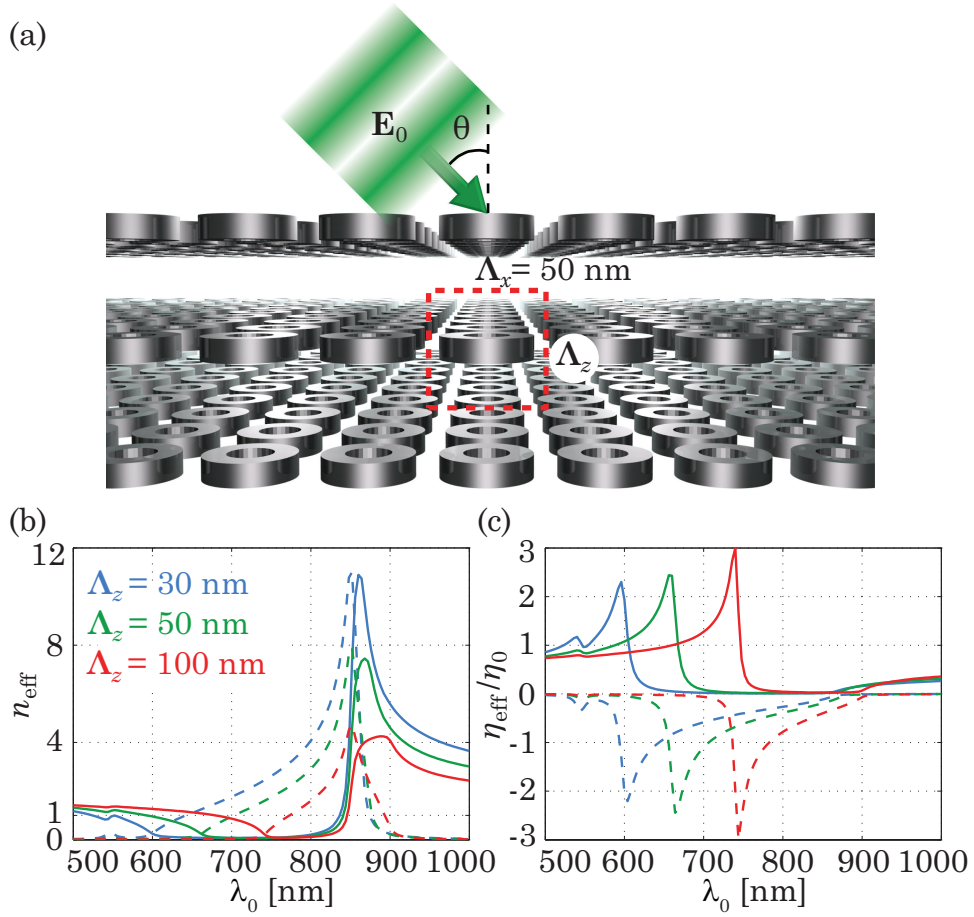

Figure 4.7. (a) Illustration of a nanomaterial composed of silver nanorings in a dielectric host medium (see Publication II). The calculated (b) effective refractive index and (c) wave impedance are shown for a TE-polarized wave incident at $\theta = 45°$. The material parameters are shown for three different lengths of the unit cell along the ring axis: $\Lambda_z = 30$ nm (blue lines), $\Lambda_z = 50$ nm (green lines) and $\Lambda_z = 100$ nm (red lines). The real and imaginary parts are shown by solid and dashed lines, respectively. The plotted wave impedances are normalized to that of vacuum.

pling between the layers may take place and it will not be possible to introduce unambiguous material parameters for the most of the relevant metamaterial designs; either these parameters will depend on the material thickness or the material thickness will be too large for obtaining any reasonably high optical transmission by the material. On the other hand, Λ_z should be chosen small compared with the wavelength. Otherwise the resulting crystal cannot be considered as homogeneous.

In order to demonstrate the influence of Λ_z on the optical properties of nanomaterials, we consider a nanomaterial composed of silver nanorings in a cubic lattice of 50 nm period, as shown in Fig. 4.7(a). This material was introduced in Publication II. The effective material parameters n_{eff} and η_{eff} are calculated by using Eqs. (3.2)-(3.5) with the coefficients τ and ρ obtained for a single two-dimensional square lattice of such nanorings.

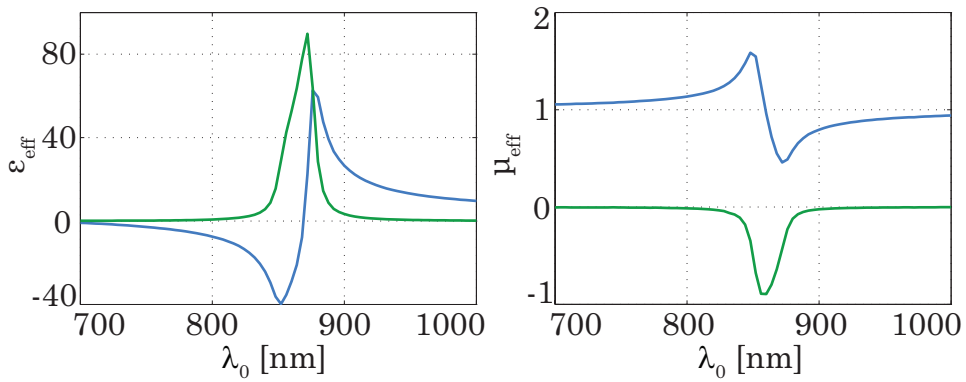

Figure 4.8. Effective relative permittivity ε_{eff} and permeability μ_{eff} for the nanoring material of Fig. 4.7 with $\Lambda_z = 50$ nm. These parameters describe the particular optical response of the medium to a TE-polarized wave incident at $\theta = 45°$. The real and imaginary parts are denoted by blue and green lines, respectively.

If the longitudinal period Λ_z changes, n_{eff} and η_{eff} change as well. For the particular choices of $\Lambda_z = 30$, 50 and 100 nm, the spectra of the parameters n_{eff} and η_{eff} are shown in Figs. 4.7(b) and 4.7(c), respectively. The wave is assumed to be TE-polarized and propagating at $\theta = 45°$ in the host medium of refractive index 1.5. As seen from Fig. 4.7(b), a smaller Λ_z provides a stronger modification of the refractive index. This is a direct consequence of the increased density of nanoscatterers. The wave impedance, shown in Fig. 4.7(c), red-shifts significantly with increasing Λ_z, which can be used to adjust the impedance at a specified wavelength. The nanorings exhibit an electric-dipole resonance at $\lambda_0 = 810$ nm, which strongly influences both n_{eff} and η_{eff} for all choices of Λ_z. It can be verified that in the spectral range from 600 to 1000 nm, all higher-order multipoles are negligible in the nanorings and, consequently, the equality $\tau \simeq 1+\rho$ holds. A relatively weak electric quadrupole resonance appears at $\lambda_0 = 550$ nm, which slightly modifies the material parameters at this wavelength. For $\Lambda_z = 50$ nm, the nanomaterial is nearly perfectly matched to air in both n_{eff} and η_{eff} at $\lambda_0 = 590$ nm. At this wavelength the electric dipole excitations in the nanorings oscillate out-of-phase with the incident field, effectively canceling the field scattered by the host medium. Also for $\Lambda_z = 30$ and 100 nm, a decent refractive index and impedance matching occurs at $\lambda_0 = 524$ and 680 nm, respectively.

The refractive index and wave impedance evaluated for various wavelengths, propagation directions and polarizations completely characterize the nanomaterial. However, one may also formally introduce the effective relative permittivity $\varepsilon_{\text{eff}} = n_{\text{eff}}\eta_0/\eta_{\text{eff}}$ and permeability $\mu_{\text{eff}} = n_{\text{eff}}\eta_{\text{eff}}/\eta_0$. For a cubic lattice of nanorings ($\Lambda_z = 50$ nm), the calculated ε_{eff} and μ_{eff}

are shown in Fig. 4.8. We notice that even though the nanorings are strictly electric dipolar scatterers, the effective permeability is modified around the dipole resonance. This result is in conflict with the idea that $\mu_{\text{eff}} \neq 1$ must be related to the excitation of magnetic dipoles. Furthermore, μ_{eff} shows an anti-resonant behavior with the imaginary part being negative at the resonance. Obviously, the fact that μ_{eff} differs from unity originates from the finite size of the unit cell and from the ensuing impossibility to treat the material as an ordinary homogeneous material free from spatial dispersion [174]. On the other hand, for designing a nanomaterial that exhibits higher-order multipole excitations, one cannot use unit cells much smaller than considered here. When the size of the scatterer approaches the quasi-static limit, the fields created by higher-order multipoles, including the magnetic dipole, become negligible compared to the electric-dipole field. One can therefore conclude that ε_{eff} and μ_{eff} are redundant parameters that do not always accurately reflect the microscopic multipole response of a nanomaterial.

The nanoring material is quite simple due to the centrosymmetric geometry of the nanoscatterers and the absence of higher-order multipole excitations. More complex nanomaterials can be created, e.g., by breaking the centrosymmetry. The nanodimer considered previously is a non-centrosymmetric scatterer that can be used to construct optically bifacial nanomaterials. In Publication V, we have considered nanodimers that are larger than the ones in Fig. 4.5 and are made of gold instead of silver. A larger size was chosen in order to enhance the contribution of the current quadrupoles and, consequently, make the material more bifacial. The radii of the two discs are now 20 and 30 nm. Both discs have a thickness of 20 nm and they are separated by a gap of 20 nm. In the nanomaterial, the nanodimers are assembled in a cubic lattice of period $\Lambda = 150$ nm. The host medium has a refractive index of 1.5. Since the effective material parameters are spatially dispersive, we separately considered the parameters n_{eff} and η_{eff} for different propagation directions. The calculated parameters are shown in Fig. 4.9.

The fact that both n_{eff} and η_{eff} depend on the light propagation direction leads to some interesting optical properties for the nanomaterial. For example, the nanomaterial can be impedance-matched to a desired medium for a desired direction of light propagation. Thus, Figs. 4.9(c) and 4.9(d) show that illumination of a nanomaterial slab from the smaller-disc side ($\theta = 0$) would yield no reflection at $\lambda_0 \approx 650$ and 630 nm at an interface

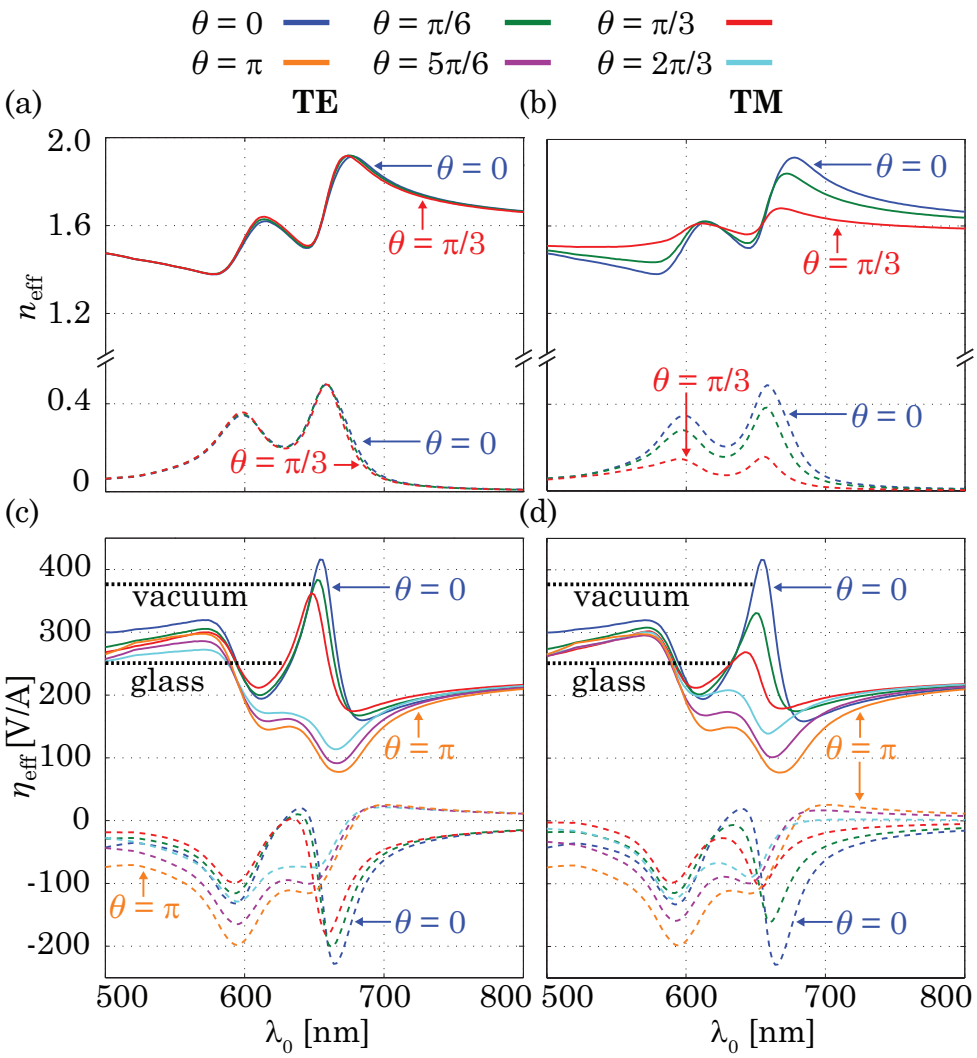

Figure 4.9. Effective material parameters n_{eff} and η_{eff} for a bifacial nanomaterial composed of gold nanodimers (see text). The different colors correspond to different angles of incidence of light propagating in the host medium of $n = 1.5$. The parameters are shown separately for (a,c) TE polarization and (b,d) TM polarization. The real and imaginary parts are denoted by solid and dashed lines, respectively. Adapted from Publication V.

of the material with air and glass, respectively. However, for illumination from the larger-disc side, significant reflection will be observed at these wavelengths due to a large impedance mismatch. In principle, one can construct a nanomaterial crystal for which different crystal cuts are impedance-matched to different materials, e.g., one to air and the opposite one to that of the used substrate.

The dependence of the refractive index on the light propagation direction means that the refraction of an *optical beam* does not obey Snell's law. Indeed, any beam can be considered as a superposition of plane waves propagating in different directions. Then, even a small difference between the refractive indices that these plane-wave components experience can change the effective refraction of the beam. As can be seen

from Figs. 4.9(a) and 4.9(b), the refractive index can either increase or decrease with an increasing angle of incidence. One could therefore obtain even negative refraction for a beam by properly designing the spatial dispersion. In essence, the spatial dispersion can alter the optical properties of a nanomaterial in ways that are not possible in conventional homogeneous materials.

5. Conclusions and outlook

In this thesis, we have developed a versatile theoretical basis for designing the optical properties of artificial nanomaterials. As spatial dispersion and higher-order multipoles are often unavoidable in realistic designs of such materials, we have appropriately taken into account their influence. Our work is therefore expected to be of importance for the development of optical nanomaterials in which these effects are considerable. Furthermore, in order to facilitate the practical applications of the presented theory, the equations in this thesis and the related publications are given in forms that can easily be implemented in numerical calculations.

In the description introduced here, both the microscopic and macroscopic aspects of optical nanomaterials are considered. On the microscopic scale, we use a specific electromagnetic multipole expansion to completely characterize the optical response of the nanomaterial's "atoms". The coefficients of the expansion reveal the actual electric current excitations in the particles, which can be exploited to design the unit cells of the material (Publication I). On the macroscopic scale, nanomaterials are characterized by spatially dispersive effective material parameters. We show that these parameters are directly linked to the transmission and reflection coefficients of the planar arrays of nanoscatterers that compose the medium (Publication II). Furthermore, these transmission and reflection coefficients can be expressed in terms of the multipole excitations in the material's unit cells. Thus, our description provides the intricate connection between the microscopic and macroscopic optical properties of nanomaterials.

We have theoretically demonstrated a surprising phenomenon in which light interacts with a subwavelength-sized pair of nanodiscs without exciting any electric dipole moment in it (Publication III). Instead, this nanodimer scatters light as a pure current quadrupole. In order to character-

ize the nanodimer, we have calculated multipole polarizabilities that describe the nanodimer's scattering properties for any propagation direction and polarization of incident light (Publication IV). The polarizabilities calculated also reveal the bifacial nature of the dimers, i.e., the multipoles excited in the particle by counter-propagating waves are different. Using this fact, we have designed an optically bifacial nanomaterial out of gold nanodimers (Publication V). For its description, we have developed a technique for obtaining the effective material parameters of spatially dispersive non-centrosymmetric media and have applied it to the nanodimer material. We show that for two counter-propagating waves with the same polarization, the wave impedances can be different, but the refractive indices are always equal.

Spatial dispersion provides optical nanomaterials with a unique sensitivity to the light propagation direction. Consequently, optical beams propagating in such materials are not expected to obey Snell's law, nor are they expected to diverge as in natural homogeneous media. An interesting question is then, to which extent the refraction and beam divergence can be controlled by employing spatially dispersive nanomaterials. Moreover, the effect of spatial dispersion depends not only on the orientation of the individual nanoscatterer, but also on the chosen configuration of the lattice. Thus, the influence of the mutual orientation of the nanoscatterers and the unit cells should be further investigated. In principle, the spatial dispersion could be specially tailored by properly breaking the symmetries of the material's unit cell. It would also be interesting to investigate the impact of spatial dispersion on optical cloaking that is routinely considered without taking this effect into account.

The developed interferometric theory for optical nanomaterials implies that, in the absence of evanescent-wave coupling between neighboring layers of nanoparticles, the effective material parameters are independent of the mutual alignment of the layers. This would provide a clear advantage for the bottom-up fabrication of optical nanomaterials, as the nanoscatterer layers could be deposited on top of each other without requiring the neighboring layers to be perfectly aligned with each other. An experimental verification of the interferometric theory and the assessment of the role of the evanescent-wave coupling is currently in progress.

It is evident that a comprehensive description of artificial optical media requires advanced theoretical methods. The multipole theory and the interferometric description presented here form a solid basis for examin-

ing the fundamental properties of optical nanomaterials. With this basis at hand, we have obtained a powerful tool for designing these materials, and are thereby one step closer to the practical realization of a variety of functional optical nanomaterials and the astonishing applications that can come along with them.

Bibliography

[1] L. D. Landau and E. M. Lifshitz, *Electrodynamics of Continuous Media* (Pergamon Press, Oxford, 1984), 2nd edition.

[2] V. G. Veselago, "The electrodynamics of substances with simultaneously negative values of ϵ and μ", *Sov. Phys. Usp.* **10**, 509–514 (1968), doi:10.1070/PU1968v010n04ABEH003699.

[3] J. B. Pendry, "Negative refraction makes a perfect lens", *Phys. Rev. Lett.* **85**, 3966–3969 (2000), doi:10.1103/PhysRevLett.85.3966.

[4] U. Leonhardt, "Optical conformal mapping", *Science* **312**, 1777–1780 (2006), doi:10.1126/science.1126493.

[5] J. B. Pendry, D. Schurig and D. R. Smith, "Controlling electromagnetic fields", *Science* **312**, 1780–1782 (2006), doi:10.1126/science.1125907.

[6] D. J. Cho, F. Wang, X. Zhang and Y. R. Shen, "Contribution of the electric quadrupole resonance in optical metamaterials", *Phys. Rev. B* **78**, 121101 (2008), doi:10.1103/PhysRevB.78.121101.

[7] B. Kante, K. O'Brien, A. Niv, X. Yin and X. Zhang, "Proposed isotropic negative index in three-dimensional optical metamaterials", *Phys. Rev. B* **85**, 041103 (2012), doi:10.1103/PhysRevB.85.041103.

[8] C. Menzel, T. Paul, C. Rockstuhl, T. Pertsch, S. Tretyakov and F. Lederer, "Validity of effective material parameters for optical fishnet metamaterials", *Phys. Rev. B* **81**, 035320 (2010), doi:10.1103/PhysRevB.81.035320.

[9] C. Menzel, C. Helgert, J. Üpping, C. Rockstuhl, E.-B. Kley, R. B. Wehrspohn, T. Pertsch and F. Lederer, "Angular resolved effective optical properties of a Swiss cross metamaterial", *Appl. Phys. Lett.* **95**, 131104 (2009), doi:10.1063/1.3238554.

[10] B. Gompf, J. Braun, T. Weiss, H. Giessen, M. Dressel and U. Hübner, "Periodic nanostructures: Spatial dispersion mimics chirality", *Phys. Rev. Lett.* **106**, 185501 (2011), doi:10.1103/PhysRevLett.106.185501.

[11] B. Gompf, B. Krausz, B. Frank and M. Dressel, "k-dependent optics of nanostructures: Spatial dispersion of metallic nanorings and split-ring resonators", *Phys. Rev. B* **86**, 075462 (2012), doi:10.1103/PhysRevB.86.075462.

[12] C. Menzel, C. Rockstuhl, T. Paul, F. Lederer and T. Pertsch, "Retrieving effective parameters for metamaterials at oblique incidence", *Phys. Rev. B* **77**, 195328 (2008), doi:10.1103/PhysRevB.77.195328.

[13] C. F. Bohren and D. R. Huffman, *Absorption and Scattering of Light by Small Particles* (Wiley, New York, 1983).

[14] E. D. Palik, *Handbook of Optical Constants of Solids* (Elsevier, 1998), available at: `http://app.knovel.com/hotlink/toc/id:kpHOCS000M/handbook-optical-constants` (visited at 19.11.2013).

[15] D. R. Lide, *CRC Handbook of Chemistry and Physics* (CRC Press, Boca Raton, 1996), 77th edition.

[16] P. B. Johnson and R. W. Christy, "Optical constants of the noble metals", *Phys. Rev. B* **6**, 4370–4379 (1972), doi:10.1103/PhysRevB.6.4370.

[17] P. B. Johnson and R. W. Christy, "Optical constants of transition metals: Ti, V, Cr, Mn, Fe, Co, Ni, and Pd", *Phys. Rev. B* **9**, 5056–5070 (1974), doi:10.1103/PhysRevB.9.5056.

[18] A. D. Rakić, "Algorithm for the determination of intrinsic optical constants of metal films: application to aluminum", *Appl. Opt.* **34**, 4755–4767 (1995), doi:10.1364/AO.34.004755.

[19] A. D. Rakić, A. B. Djurišic, J. M. Elazar and M. L. Majewski, "Optical properties of metallic films for vertical-cavity optoelectronic devices", *Appl. Opt.* **37**, 5271–5283 (1998), doi:10.1364/AO.37.005271.

[20] J. D. Jackson, *Classical Electrodynamics* (Wiley, New York, 1999), 3rd edition.

[21] H. Kragh, "Ludvig Lorenz and nineteenth century optical theory: the work of a great Danish scientist", *Appl. Opt.* **30**, 4688–4695 (1991), doi:10.1364/AO.30.004688.

[22] P. Lilienfeld, "Gustav Mie: the person", *Appl. Opt.* **30**, 4696–4698 (1991), doi:10.1364/AO.30.004696.

[23] C. Mätzler, "MATLAB functions for Mie scattering and absorption, version 2", in "IAP Research Report", (University of Bern, 2002), available at: `http://www.iap.unibe.ch/publications` (visited at 19.11.2013).

[24] O. Peña and U. Pal, "Scattering of electromagnetic radiation by a multilayered sphere", *Comput. Phys. Commun.* **180**, 2348–2354 (2009), doi:10.1016/j.cpc.2009.07.010, code available at `http://cpc.cs.qub.ac.uk/cpc/cgi-bin/showversions.pl/?catid=AEEY` (visited at 19.11.2013).

[25] S. Asano and G. Yamamoto, "Light scattering by a spheroidal particle", *Appl. Opt.* **14**, 29–49 (1975), doi:10.1364/AO.14.000029.

[26] S. Asano, "Light scattering properties of spheroidal particles", *Appl. Opt.* **18**, 712–723 (1979), doi:10.1364/AO.18.000712.

[27] V. G. Farafonov, N. V. Voshchinnikov and V. V. Somsikov, "Light scattering by a core-mantle spheroidal particle", *Appl. Opt.* **35**, 5412–5426 (1996), doi:10.1364/AO.35.005412.

[28] I. Gurwich, M. Kleiman, N. Shiloah and A. Cohen, "Scattering of electromagnetic radiation by multilayered spheroidal particles: Recursive procedure", *Appl. Opt.* **39**, 470–477 (2000), doi:10.1364/AO.39.000470.

[29] V. G. Farafonov and N. V. Voshchinnikov, "Light scattering by a multilayered spheroidal particle", *Appl. Opt.* **51**, 1586–1597 (2012), doi:10.1364/AO.51.001586.

[30] F. Kahnert, "Numerical methods in electromagnetic scattering theory", *J. Quant. Spectrosc. Radiat. Transfer* **79-80**, 775–824 (2003), doi:10.1016/S0022-4073(02)00321-7.

[31] Y. Zhu and A. C. Cangellaris, *Multigrid Finite Element Methods for Electromagnetic Field Modeling* (IEEE Press, New Jersey, 2006).

[32] A. Taflove and S. C. Hagness, *Computational Electrodynamics: The Finite-Difference Time-Domain Method* (Artech House, Boston, 2005), 3rd edition.

[33] ANSYS HFSS, `http://www.ansys.com` (visited at 19.11.2013).

[34] COMSOL Multiphysics, `http://www.comsol.com/` (visited at 19.11.2013).

[35] CST MICROWAVE STUDIO, `https://www.cst.com/Products/CSTMWS` (visited at 19.11.2013).

[36] EM Explorer, `http://www.emexplorer.net/` (visited at 19.11.2013).

[37] JCMsuite, `http://www.jcmwave.com/` (visited at 19.11.2013).

[38] Lumerical FDTD Solutions, `http://www.lumerical.com/` (visited at 19.11.2013).

[39] OmniSim, `http://www.photond.com/products/omnisim.htm` (visited at 19.11.2013).

[40] OptiFDTD, `http://optiwave.com/category/products/component-design/optifdtd` (visited at 19.11.2013).

[41] RSoft CAD Environment, `http://optics.synopsys.com/rsoft/rsoft-cad-environment.html` (visited at 19.11.2013).

[42] SEMCAD X, `http://www.speag.com/products/semcad` (visited at 19.11.2013).

[43] Remcom XFdtd, `http://www.remcom.com/xf7` (visited at 19.11.2013).

[44] A. F. Oskooi, D. Roundy, M. Ibanescu, P. Bermel, J. D. Joannopoulos and S. G. Johnson, "MEEP: A flexible free-software package for electromagnetic simulations by the FDTD method", *Comput. Phys. Commun.* **181**, 687–702 (2010), doi:10.1016/j.cpc.2009.11.008, program available at `http://ab-initio.mit.edu/meep` (visited at 19.11.2013).

[45] I. R. Capoglu, "Angora, a free finite-difference time-domain (FDTD) electromagnetic simulation package", program available at `http://www.angorafdtd.org/` (visited at 19.11.2013).

[46] B. T. Draine and P. J. Flatau, “Discrete-dipole approximation for scattering calculations”, *J. Opt. Soc. Am. A* **11**, 1491–1499 (1994), doi:10.1364/JOSAA.11.001491, program available at `http://www.astro.princeton.edu/~draine/DDSCAT.html` (visited at 19.11.2013).

[47] M. A. Yurkin and A. G. Hoekstra, “The discrete-dipole-approximation code ADDA: Capabilities and known limitations”, *J. Quant. Spectrosc. Radiat. Transfer* **112**, 2234–2247 (2011), doi:10.1016/j.jqsrt.2011.01.031, program available at `http://code.google.com/p/a-dda` (visited at 19.11.2013).

[48] J. Hoffmann, C. Hafner, P. Leidenberg, J. Hesselbarth and S. Burger, “Comparison of electromagnetic field solvers for the 3D analysis of plasmonic nanoantennas”, *Proc. SPIE* **7390**, 73900J (2009), doi:10.1117/12.828036.

[49] T. Feichtner, O. Selig, M. Kiunke and B. Hecht, “Evolutionary optimization of optical antennas”, *Phys. Rev. Lett.* **109**, 127701 (2012), doi:10.1103/PhysRevLett.109.127701.

[50] J. He, A. Karlsson, J. Swartling and S. Andersson-Engels, “Light scattering by multiple red blood cells”, *J. Opt. Soc. Am. A* **21**, 1953–1961 (2004), doi:10.1364/JOSAA.21.001953.

[51] E. Semouchkina, D. H. Werner, G. B. Semouchkin and C. Pantano, “An infrared invisibility cloak composed of glass”, *Appl. Phys. Lett.* **96**, 233503 (2010), doi:10.1063/1.3447794.

[52] S. Tanev, W. Sun, R. Zhang and A. Ridsdale, “The FDTD approach applied to light scattering from single biological cells”, *Proc. SPIE* **5474**, 162 (2003), doi:10.1117/12.578382.

[53] L. Zhou, Q. Gan, F. J. Bartoli and V. Dierolf, “Direct near-field optical imaging of UV bowtie nanoantennas”, *Opt. Express* **17**, 20301–20306 (2009), doi:10.1364/OE.17.020301.

[54] H. P. Paudel, M. F. Baroughi and K. Bayat, “Plasmon resonance modes in two-dimensional arrays of metallic nanopillars”, *J. Opt. Soc. Am. B* **27**, 1693–1697 (2010), doi:10.1364/JOSAB.27.001693.

[55] J. T. Krug II, E. J. Sánchez and X. S. Xie, “Design of near-field optical probes with optimal field enhancement by finite difference time domain electromagnetic simulation”, *J. Chem. Phys.* **116**, 10895–10901 (2002), doi:10.1063/1.1479723.

[56] W. H. P. Pernice, F. P. Payne and D. F. G. Gallagher, “Numerical investigation of field enhancement by metal nano-particles using a hybrid FDTD-PSTD algorithm”, *Opt. Express* **15**, 11433–11443 (2007), doi:10.1364/OE.15.011433.

[57] S. Link and M. A. El-Sayed, “Optical properties and ultrafast dynamics of metallic nanocrystals”, *Annu. Rev. Phys. Chem.* **54**, 331–366 (2003), doi:10.1146/annurev.physchem.54.011002.103759.

[58] P. N. Prasad, *Nanophotonics* (Wiley, New Jersey, 2004).

[59] G. Sun and J. B. Khurgin, “Plasmonic enhancement of optical properties by isolated and coupled metal nanoparticles”, in G. Shvets and I. Tsukerman, editors, “Plasmonics and Plasmonic Metamaterials”, (World Scientific Publishing, Singapore, 2012).

[60] R. Filter, S. Mühlig, T. Eichelkraut, C. Rockstuhl and F. Lederer, "Controlling the dynamics of quantum mechanical systems sustaining dipole-forbidden transitions via optical nanoantennas", *Phys. Rev. B* **86**, 035404 (2012), doi:10.1103/PhysRevB.86.035404.

[61] A. J. Haes, W. P. Hall, L. Chang, W. L. Klein and R. P. Van Duyne, "A localized surface plasmon resonance biosensor: First steps toward an assay for Alzheimer's disease", *Nano Lett.* **4**, 1029–1034 (2004), doi:10.1021/nl049670j.

[62] P. K. Jain, X. Huang, I. H. El-Sayed and M. A. El-Sayed, "Review of some interesting surface plasmon resonance-enhanced properties of noble metal nanoparticles and their applications to biosystems", *Plasmonics* **2**, 107–118 (2007), doi:10.1007/s11468-007-9031-1.

[63] S. Lee, K. M. Mayer and J. H. Hafner, "Improved localized surface plasmon resonance immunoassay with gold bipyramid substrates", *Anal. Chem.* **81**, 4450–4455 (2009), doi:10.1021/ac900276n.

[64] H. Altug, A. A. Yanik, R. Adato, S. Aksu, A. Artar and M. Huang, "Plasmonics for ultrasensitive nanospectroscopy and optofluidic-plasmonics biosensors", in G. Shvets and I. Tsukerman, editors, "Plasmonics and Plasmonic Metamaterials", (World Scientific Publishing, Singapore, 2012).

[65] U. Kreibig and M. Vollmer, *Optical Properties of Metal Clusters* (Springer, Berlin, 1995).

[66] L. Novotny and B. Hecht, *Principles of Nano-Optics* (Cambridge University Press, Cambridge, 2012), 2nd edition.

[67] R. H. Lambert, "Complete vector spherical harmonic expansion for Maxwell's equations", *Am. J. Phys.* **46**, 849–852 (1978), doi:10.1119/1.11202.

[68] L. Zhao, K. L. Kelly and G. C. Schatz, "The extinction spectra of silver nanoparticle arrays: Influence of array structure on plasmon resonance wavelength and width", *J. Phys. Chem. B* **107**, 7343–7350 (2003), doi:10.1021/jp034235j.

[69] S. Zou and G. C. Schatz, "Narrow plasmonic/photonic extinction and scattering line shapes for one and two dimensional silver nanoparticle arrays", *J. Chem. Phys.* **121**, 12606–12612 (2004), doi:10.1063/1.1826036.

[70] S. Biring, H.-H. Wang, J.-K. Wang and Y.-L. Wang, "Light scattering from 2D arrays of monodispersed Ag-nanoparticles separated by tunable nanogaps: spectral evolution and analytical analysis of plasmonic coupling", *Opt. Express* **16**, 15312–15324 (2008), doi:10.1364/OE.16.015312.

[71] B. Auguié and W. L. Barnes, "Collective resonances in gold nanoparticle arrays", *Phys. Rev. Lett.* **101**, 143902 (2008), doi:10.1103/PhysRevLett.101.143902.

[72] A. I. Väkeväinen, R. J. Moerland, H. T. Rekola, A.-P. Eskelinen, J.-P. Martikainen, D.-H. Kim and P. Törmä, "Plasmonic surface lattice resonances at the strong coupling regime", accepted by *Nano Lett.* (2013), doi:10.1021/nl4035219.

[73] F. J. García de Abajo, "*Colloquium*: Light scattering by particle and hole arrays", *Rev. Mod. Phys.* **79**, 1267–1290 (2007), doi:10.1103/RevModPhys.79.1267.

[74] V. G. Kravets, F. Schedin and A. N. Grigorenko, "Extremely narrow plasmon resonances based on diffraction coupling of localized plasmons in arrays of metallic nanoparticles", *Phys. Rev. Lett.* **101**, 087403 (2008), doi:10.1103/PhysRevLett.101.087403.

[75] R. Kullock, S. Grafström, P. R. Evans, R. J. Pollard and L. M. Eng, "Metallic nanorod arrays: negative refraction and optical properties explained by retarded dipolar interactions", *J. Opt. Soc. Am. B* **27**, 1819–1827 (2010), doi:10.1364/JOSAB.27.001819.

[76] A. B. Evlyukhin, C. Reinhardt, U. Zywietz and B. N. Chichkov, "Collective resonances in metal nanoparticle arrays with dipole-quadrupole interactions", *Phys. Rev. B* **85**, 245411 (2012), doi:10.1103/PhysRevB.85.245411.

[77] M. Meier, A. Wokaun and P. F. Liao, "Enhanced fields on rough surfaces: dipolar interactions among particles of sizes exceeding the Rayleigh limit", *J. Opt. Soc. Am. B* **2**, 931–949 (1985), doi:10.1364/JOSAB.2.000931.

[78] A. Boltasseva and V. M. Shalaev, "Fabrication of optical negative-index metamaterials: Recent advances and outlook", *Metamaterials* **2**, 1–17 (2008), doi:10.1016/j.metmat.2008.03.004.

[79] D. Schurig, J. J. Mock, B. J. Justice, S. A. Cummer, J. B. Pendry, A. F. Starr and D. R. Smith, "Metamaterial electromagnetic cloak at microwave frequencies", *Science* **314**, 977–980 (2006), doi:10.1126/science.1133628.

[80] R. Liu, C. Ji, J. J. Mock, J. Y. Chin, T. J. Cui and D. R. Smith, "Broadband ground-plane cloak", *Science* **323**, 366–369 (2009), doi:10.1126/science.1166949.

[81] J. Perczel, T. Tyc and U. Leonhardt, "Invisibility cloaking without superluminal propagation", *New J. Phys.* **13**, 083007 (2011), doi:10.1088/1367-2630/13/8/083007.

[82] S. Xu, X. Cheng, S. Xi, R. Zhang, H. O. Moser, Z. Shen, Y. Xu, Z. Huang, X. Zhang, F. Yu, B. Zhang and H. Chen, "Experimental demonstration of a free-space cylindrical cloak without superluminal propagation", *Phys. Rev. Lett.* **109**, 223903 (2012), doi:10.1103/PhysRevLett.109.223903.

[83] Y. Urzhumov and D. R. Smith, "Low-loss directional cloaks without superluminal velocity or magnetic response", *Opt. Lett.* **37**, 4471–4473 (2012), doi:10.1364/OL.37.004471.

[84] R. Zhao, Th. Koschny, E. N. Economou and C. M. Soukoulis, "Comparison of chiral metamaterial designs for repulsive Casimir force", *Phys. Rev. B* **81**, 235126 (2010), doi:10.1103/PhysRevB.81.235126.

[85] R. Zhao, Th. Koschny, E. N. Economou and C. M. Soukoulis, "Repulsive Casimir forces with finite-thickness slabs", *Phys. Rev. B* **83**, 075108 (2011), doi:10.1103/PhysRevB.83.075108.

[86] S. Zhang, D. A. Genov, Y. Wang, M. Liu and X. Zhang, "Plasmon-induced transparency in metamaterials", *Phys. Rev. Lett.* **101**, 047401 (2008), doi:10.1103/PhysRevLett.101.047401.

[87] S. I. Bozhevolnyi, A. B. Evlyukhin, A. Pors, M. G. Nielsen, M. Willatzen and O. Albrektsen, "Optical transparency by detuned electrical dipoles", *New J. Phys.* **13**, 023034 (2011), doi:10.1088/1367-2630/13/2/023034.

[88] Z. Jacob, L. V. Alekseyev and E. Narimanov, "Optical hyperlens: Far-field imaging beyond the diffraction limit", *Opt. Express* **14**, 8247–8256 (2006), doi:10.1364/OE.14.008247.

[89] I. I. Smolyaninov, Y.-J. Hung and C. C. Davis, "Magnifying superlens in the visible frequency range", *Science* **315**, 1699–1701 (2007), doi:10.1126/science.1138746.

[90] Z. Liu, H. Lee, Y. Xiong, C. Sun and X. Zhang, "Far-field optical hyperlens magnifying sub-diffraction-limited objects", *Science* **315**, 1686 (2007), doi:10.1126/science.1137368.

[91] J. Rho, Z. Ye, Y. Xiong, X. Yin, Z. Liu, H. Choi, G. Bartal and X. Zhang, "Spherical hyperlens for two-dimensional sub-diffractional imaging at visible frequencies", *Nat. Commun.* **1**, 143 (2010), doi:10.1038/ncomms1148.

[92] C. Ma and Z. Liu, "Focusing light into deep subwavelength using metamaterial immersion lenses", *Opt. Express* **18**, 4838–4844 (2010), doi:10.1364/OE.18.004838.

[93] D. Lu and Z. Liu, "Hyperlenses and metalenses for far-field super-resolution imaging", *Nat. Commun.* **3**, 1205 (2012), doi:10.1038/ncomms2176.

[94] T. Roy, E. T. F. Rogers and N. I. Zheludev, "Sub-wavelength focusing metalens", *Opt. Express* **21**, 7577–7582 (2013), doi:10.1364/OE.21.007577.

[95] C. Argyropoulos, N. M. Estakhri, F. Monticone and A. Alù, "Negative refraction, gain and nonlinear effects in hyperbolic metamaterials", *Opt. Express* **21**, 15037–15047 (2013), doi:10.1364/OE.21.015037.

[96] T. Zhang, L. Chen and X. Li, "Graphene-based tunable broadband hyperlens for far-field subdiffraction imaging at mid-infrared frequencies", *Opt. Express* **21**, 20888–20899 (2013), doi:10.1364/OE.21.020888.

[97] H. Y. Dong, J. Wang, K. H. Fung and T. J. Cui, "Super-resolution image transfer by a vortex-like metamaterial", *Opt. Express* **21**, 9407–9413 (2013), doi:10.1364/OE.21.009407.

[98] B. Walther, C. Helgert, C. Rockstuhl and T. Pertsch, "Diffractive optical elements based on plasmonic metamaterials", *Appl. Phys. Lett.* **98**, 191101 (2011), doi:10.1063/1.3587622.

[99] B. Walther, C. Helgert, C. Rockstuhl, F. Setzpfandt, F. Eilenberger, E.-B. Kley, F. Lederer, A. Tünnermann and T. Pertsch, "Spatial and spectral light shaping with metamaterials", *Adv. Mater.* **24**, 6300–6304 (2012), doi:10.1002/adma.201202540.

[100] F. Aieta, P. Genevet, M. A. Kats, N. Yu, R. Blanchard, Z. Gaburro and F. Capasso, "Aberration-free ultrathin flat lenses and axicons at telecom wavelengths based on plasmonic metasurfaces", *Nano Lett.* **12**, 4932–4936 (2012), doi:10.1021/nl302516v.

[101] X. Zhang and Y. Chen, "Broadband phase retarder based on one-dimensional photonic crystal containing mu-negative materials", *J. Opt. Soc. Am. B* **29**, 2704–2709 (2012), doi:10.1364/JOSAB.29.002704.

[102] M. M. I. Saadoun and N. Engheta, "A reciprocal phase shifter using novel pseudochiral or ω medium", *Microw. Opt. Tech. Lett.* **5**, 184–188 (1992), doi:10.1002/mop.4650050412.

[103] A. V. Kildishev, A. Boltasseva and V. M. Shalaev, "Planar photonics with metasurfaces", *Science* **339** (2013), doi:10.1126/science.1232009.

[104] T. Roy, A. E. Nikolaenko and E. T. F. Rogers, "A meta-diffraction-grating for visible light", *J. Opt.* **15**, 085101 (2013), doi:10.1088/2040-8978/15/8/085101.

[105] Y. Sun, B. Edwards, A. Alù and N. Engheta, "Experimental realization of optical lumped nanocircuits at infrared wavelengths", *Nature Mater.* **11**, 208–212 (2012), doi:10.1038/nmat3230.

[106] U. K. Chettiar and N. Engheta, "Optical frequency mixing through nanoantenna enhanced difference frequency generation: Metatronic mixer", *Phys. Rev. B* **86**, 075405 (2012), doi:10.1103/PhysRevB.86.075405.

[107] H. Caglayan, S.-H. Hong, B. Edwards, C. R. Kagan and N. Engheta, "Near-infrared metatronic nanocircuits by design", *Phys. Rev. Lett.* **111**, 073904 (2013), doi:10.1103/PhysRevLett.111.073904.

[108] V. Mocella, S. Cabrini, A. S. P. Chang, P. Dardano, L. Moretti, I. Rendina, D. Olynick, B. Harteneck and S. Dhuey, "Self-collimation of light over millimeter-scale distance in a quasi-zero-average-index metamaterial", *Phys. Rev. Lett.* **102**, 133902 (2009), doi:10.1103/PhysRevLett.102.133902.

[109] C. M. Watts, X. Liu and W. J. Padilla, "Metamaterial electromagnetic wave absorbers", *Adv. Mater.* **24**, OP98–OP120 (2012), doi:10.1002/adma.201200674.

[110] Z. Liu, X. Zhang, Y. Mao, Y. Y. Zhu, Z. Yang, C. T. Chan and P. Sheng, "Locally resonant sonic materials", *Science* **289**, 1734–1736 (2000), doi:10.1126/science.289.5485.1734.

[111] J. Li and C. T. Chan, "Double-negative acoustic metamaterial", *Phys. Rev. E* **70**, 055602 (2004), doi:10.1103/PhysRevE.70.055602.

[112] H. Chen and C. T. Chan, "Acoustic cloaking in three dimensions using acoustic metamaterials", *Appl. Phys. Lett.* **91**, 183518 (2007), doi:10.1063/1.2803315.

[113] M. Ambati, N. Fang, C. Sun and X. Zhang, "Surface resonant states and superlensing in acoustic metamaterials", *Phys. Rev. B* **75**, 195447 (2007), doi:10.1103/PhysRevB.75.195447.

[114] J. Q. Quach, C.-H. Su, A. M. Martin, A. D. Greentree and L. C. L. Hollenberg, "Reconfigurable quantum metamaterials", *Opt. Express* **19**, 11018–11033 (2011), doi:10.1364/OE.19.011018.

[115] A. M. Zagoskin, "Superconducting quantum metamaterials in 3D: possible realizations", *J. Opt.* **14**, 114011 (2012), doi:10.1088/2040-8978/14/11/114011.

[116] J. Q. Quach, C.-H. Su and A. D. Greentree, "Transformation optics for cavity array metamaterials", *Opt. Express* **21**, 5575–5581 (2013), doi:10.1364/OE.21.005575.

[117] A. Shvetsov, A. M. Satanin, F. Nori, S. Savel'ev and A. M. Zagoskin, "Quantum metamaterial without local control", *Phys. Rev. B* **87**, 235410 (2013), doi:10.1103/PhysRevB.87.235410.

[118] J. B. Pendry, A. J. Holden, D. J. Robbins and W. J. Stewart, "Magnetism from conductors and enhanced nonlinear phenomena", *IEEE Trans. Microw. Theory Techn.* **47**, 2075–2084 (1999), doi:10.1109/22.798002.

[119] D. R. Smith, W. J. Padilla, D. C. Vier, S. C. Nemat-Nasser and S. Schultz, "Composite medium with simultaneously negative permeability and permittivity", *Phys. Rev. Lett.* **84**, 4184–4187 (2000), doi:10.1103/PhysRevLett.84.4184.

[120] R. A. Shelby, D. R. Smith and S. Schultz, "Experimental verification of a negative index of refraction", *Science* **292**, 77–79 (2001), doi:10.1126/science.1058847.

[121] M. Bayindir, K. Aydin, E. Ozbay, P. Markoš and C. M. Soukoulis, "Transmission properties of composite metamaterials in free space", *Appl. Phys. Lett.* **81**, 120–122 (2002), doi:10.1063/1.1492009.

[122] R. B. Greegor, C. G. Parazzoli, K. Li and M. H. Tanielian, "Origin of dissipative losses in negative index of refraction materials", *Appl. Phys. Lett.* **82**, 2356–2358 (2003), doi:10.1063/1.1563726.

[123] K. Aydin, K. Guven, M. Kafesaki, L. Zhang, C. M. Soukoulis and E. Ozbay, "Experimental observation of true left-handed transmission peaks in metamaterials", *Opt. Lett.* **29**, 2623–2625 (2004), doi:10.1364/OL.29.002623.

[124] V. M. Shalaev, "Optical negative-index metamaterials", *Nat. Photonics* **1**, 41–48 (2007), doi:10.1038/nphoton.2006.49.

[125] J. Zhou, Th. Koschny, M. Kafesaki, E. N. Economou, J. B. Pendry and C. M. Soukoulis, "Saturation of the magnetic response of split-ring resonators at optical frequencies", *Phys. Rev. Lett.* **95**, 223902 (2005), doi:10.1103/PhysRevLett.95.223902.

[126] M. W. Klein, C. Enkrich, M. Wegener, C. M. Soukoulis and S. Linden, "Single-slit split-ring resonators at optical frequencies: limits of size scaling", *Opt. Lett.* **31**, 1259–1261 (2006), doi:10.1364/OL.31.001259.

[127] A. Ishikawa, T. Tanaka and S. Kawata, "Negative magnetic permeability in the visible light region", *Phys. Rev. Lett.* **95**, 237401 (2005), doi:10.1103/PhysRevLett.95.237401.

[128] S. Linden, C. Enkrich, M. Wegener, J. Zhou, Th. Koschny and C. M. Soukoulis, "Magnetic response of metamaterials at 100 terahertz", *Science* **306**, 1351–1353 (2004), doi:10.1126/science.1105371.

[129] N. Katsarakis, G. Konstantinidis, A. Kostopoulos, R. S. Penciu, T. F. Gundogdu, M. Kafesaki, E. N. Economou, Th. Koschny and C. M. Soukoulis, "Magnetic response of split-ring resonators in the far-infrared frequency regime", *Opt. Lett.* **30**, 1348–1350 (2005), doi:10.1364/OL.30.001348.

[130] S. Zhang, W. Fan, B. K. Minhas, A. Frauenglass, K. J. Malloy and S. R. J. Brueck, "Midinfrared resonant magnetic nanostructures exhibiting a negative permeability", *Phys. Rev. Lett.* **94**, 037402 (2005), doi:10.1103/PhysRevLett.94.037402.

[131] C. Enkrich, M. Wegener, S. Linden, S. Burger, L. Zschiedrich, F. Schmidt, J. F. Zhou, Th. Koschny and C. M. Soukoulis, "Magnetic metamaterials at telecommunication and visible frequencies", *Phys. Rev. Lett.* **95**, 203901 (2005), doi:10.1103/PhysRevLett.95.203901.

[132] G. Dolling, C. Enkrich, M. Wegener, J. F. Zhou, C. M. Soukoulis and S. Linden, "Cut-wire pairs and plate pairs as magnetic atoms for optical metamaterials", *Opt. Lett.* **30**, 3198–3200 (2005), doi:10.1364/OL.30.003198.

[133] V. M. Shalaev, W. Cai, U. K. Chettiar, H.-K. Yuan, A. K. Sarychev, V. P. Drachev and A. V. Kildishev, "Negative index of refraction in optical metamaterials", *Opt. Lett.* **30**, 3356–3358 (2005), doi:10.1364/OL.30.003356.

[134] A. Ishikawa, T. Tanaka and S. Kawata, "Magnetic excitation of magnetic resonance in metamaterials at far-infrared frequencies", *Appl. Phys. Lett.* **91**, 113118 (2007), doi:10.1063/1.2785167.

[135] S. Zhang, W. Fan, N. C. Panoiu, K. J. Malloy, R. M. Osgood and S. R. J. Brueck, "Experimental demonstration of near-infrared negative-index metamaterials", *Phys. Rev. Lett.* **95**, 137404 (2005), doi:10.1103/PhysRevLett.95.137404.

[136] G. Dolling, C. Enkrich, M. Wegener, C. M. Soukoulis and S. Linden, "Low-loss negative-index metamaterial at telecommunication wavelengths", *Opt. Lett.* **31**, 1800–1802 (2006), doi:10.1364/OL.31.001800.

[137] G. Dolling, C. Enkrich, M. Wegener, C. M. Soukoulis and S. Linden, "Simultaneous negative phase and group velocity of light in a metamaterial", *Science* **312**, 892–894 (2006), doi:10.1126/science.1126021.

[138] G. Dolling, M. Wegener, C. M. Soukoulis and S. Linden, "Negative-index metamaterial at 780 nm wavelength", *Opt. Lett.* **32**, 53–55 (2007), doi:10.1364/OL.32.000053.

[139] S. P. Burgos, R. de Waele, A. Polman and H. A. Atwater, "A single-layer wide-angle negative-index metamaterial at visible frequencies", *Nature Mater.* **9**, 407–412 (2010), doi:10.1038/nmat2747.

[140] C. García-Meca, J. Hurtado, J. Martí, A. Martínez, W. Dickson and A. V. Zayats, "Low-loss multilayered metamaterial exhibiting a negative index of refraction at visible wavelengths", *Phys. Rev. Lett.* **106**, 067402 (2011), doi:10.1103/PhysRevLett.106.067402.

[141] J. Cong, B. Yun and Y. Cui, "Negative-index metamaterial at visible frequencies based on high order plasmon resonance", *Appl. Opt.* **51**, 2469–2476 (2012), doi:10.1364/AO.51.002469.

[142] M. I. Aslam and D. Ö. Güney, "Dual-band, double-negative, polarization-independent metamaterial for the visible spectrum", *J. Opt. Soc. Am. B* **29**, 2839–2847 (2012), doi:10.1364/JOSAB.29.002839.

[143] N.-H. Shen, Th. Koschny, M. Kafesaki and C. M. Soukoulis, "Optical metamaterials with different metals", *Phys. Rev. B* **85**, 075120 (2012), doi:10.1103/PhysRevB.85.075120.

[144] F. Chen, L. Yuan and R. L. Johnston, "Low-loss optical magnetic metamaterials on Ag–Au bimetallic fishnets", *J. Magn. Magn. Mater.* **324**, 2625–2630 (2012), doi:10.1016/j.jmmm.2012.03.025.

[145] K. Vynck, D. Felbacq, E. Centeno, A. I. Căbuz, D. Cassagne and B. Guizal, "All-dielectric rod-type metamaterials at optical frequencies", *Phys. Rev. Lett.* **102**, 133901 (2009), doi:10.1103/PhysRevLett.102.133901.

[146] J. C. Ginn, I. Brener, D. W. Peters, J. R. Wendt, J. O. Stevens, P. F. Hines, L. I. Basilio, L. K. Warne, J. F. Ihlefeld, P. G. Clem and M. B. Sinclair, "Realizing optical magnetism from dielectric metamaterials", *Phys. Rev. Lett.* **108**, 097402 (2012), doi:10.1103/PhysRevLett.108.097402.

[147] G. V. Naik, J. L. Schroeder, X. Ni, A. V. Kildishev, T. D. Sands and A. Boltasseva, "Titanium nitride as a plasmonic material for visible and near-infrared wavelengths", *Opt. Mater. Express* **2**, 478–489 (2012), doi:10.1364/OME.2.000478.

[148] O. Hess, J. B. Pendry, S. A. Maier, R. F. Oulton, J. M. Hamm and K. L. Tsakmakidis, "Active nanoplasmonic metamaterials", *Nature Mater.* **11**, 573–584 (2012), doi:10.1038/nmat3356.

[149] J. Yao, Z. Liu, Y. Liu, Y. Wang, C. Sun, G. Bartal, A. M. Stacy and X. Zhang, "Optical negative refraction in bulk metamaterials of nanowires", *Science* **321**, 930 (2008), doi:10.1126/science.1157566.

[150] Y. Liu, G. Bartal and X. Zhang, "All-angle negative refraction and imaging in a bulk medium made of metallic nanowires in the visible region", *Opt. Express* **16**, 15439–15448 (2008), doi:10.1364/OE.16.015439.

[151] T. Paul, C. Rockstuhl, C. Menzel and F. Lederer, "Anomalous refraction, diffraction, and imaging in metamaterials", *Phys. Rev. B* **79**, 115430 (2009), doi:10.1103/PhysRevB.79.115430.

[152] S. Yun, Z. H. Jiang, Q. Xu, Z. Liu, D. H. Werner and T. S. Mayer, "Low-loss impedance-matched optical metamaterials with zero-phase delay", *ACS Nano* **6**, 4475–4482 (2012), doi:10.1021/nn3012338.

[153] P. Moitra, Y. Yang, Z. Anderson, I. I. Kravchenko, D. P. Briggs and J. Valentine, "Realization of an all-dielectric zero-index optical metamaterial", *Nature Photon.* **7**, 791–795 (2013), doi:10.1038/nphoton.2013.214.

[154] M. Choi, S. H. Lee, Y. Kim, S. B. Kang, J. Shin, M. H. Kwak, K.-Y. Kang, Y.-H. Lee, N. Park and B. Min, "A terahertz metamaterial with unnaturally high refractive index", *Nature* **470**, 369–373 (2011), doi:10.1038/nature09776.

[155] K. Sakoda, *Optical Properties of Photonic Crystals* (Springer, Berlin, 2005), 2nd edition.

[156] D. R. Smith, S. Schultz, P. Markoš and C. M. Soukoulis, "Determination of effective permittivity and permeability of metamaterials from reflection and transmission coefficients", *Phys. Rev. B* **65**, 195104 (2002), doi:10.1103/PhysRevB.65.195104.

[157] D. R. Smith, D. C. Vier, Th. Koschny and C. M. Soukoulis, "Electromagnetic parameter retrieval from inhomogeneous metamaterials", *Phys. Rev. E* **71**, 036617 (2005), doi:10.1103/PhysRevE.71.036617.

[158] W.-C. Chen, A. Totachawattana, K. Fan, J. L. Ponsetto, A. C. Strikwerda, X. Zhang, R. D. Averitt and W. J. Padilla, "Single-layer terahertz metamaterials with bulk optical constants", *Phys. Rev. B* **85**, 035112 (2012), doi:10.1103/PhysRevB.85.035112.

[159] T. Paul, C. Menzel, W. Śmigaj, C. Rockstuhl, P. Lalanne and F. Lederer, "Reflection and transmission of light at periodic layered metamaterial films", *Phys. Rev. B* **84**, 115142 (2011), doi:10.1103/PhysRevB.84.115142.

[160] C. Rockstuhl, T. Paul, F. Lederer, T. Pertsch, T. Zentgraf, T. P. Meyrath and H. Giessen, "Transition from thin-film to bulk properties of metamaterials", *Phys. Rev. B* **77**, 035126 (2008), doi:10.1103/PhysRevB.77.035126.

[161] C. R. Simovski, "Bloch material parameters of magneto-dielectric metamaterials and the concept of Bloch lattices", *Metamaterials* **1**, 62–80 (2007), doi:10.1016/j.metmat.2007.09.002.

[162] M. Born and E. Wolf, *Principles of Optics* (Cambridge University Press, Cambridge, 1999), 7th edition.

[163] J. D. Joannopoulos, S. G. Johnson, J. N. Winn and R. D. Meade, *Photonic Crystals: Molding the Flow of Light* (Princeton University Press, New Jersey, 2008), 2nd edition.

[164] L. Li, "New formulation of the Fourier modal method for crossed surface-relief gratings", *J. Opt. Soc. Am. A* **14**, 2758–2767 (1997), doi:10.1364/JOSAA.14.002758.

[165] J. Yang, C. Sauvan, T. Paul, C. Rockstuhl, F. Lederer and P. Lalanne, "Retrieving the effective parameters of metamaterials from the single interface scattering problem", *Appl. Phys. Lett.* **97**, 061102 (2010), doi:10.1063/1.3478241.

[166] S. Mühlig, C. Menzel, C. Rockstuhl and F. Lederer, "Multipole analysis of meta-atoms", *Metamaterials* **5**, 64–73 (2011), doi:10.1016/j.metmat.2011.03.003.

[167] C. Rockstuhl, C. Menzel, S. Mühlig, J. Petschulat, C. Helgert, C. Etrich, A. Chipouline, T. Pertsch and F. Lederer, "Scattering properties of meta-atoms", *Phys. Rev. B* **83**, 245119 (2011), doi:10.1103/PhysRevB.83.245119.

[168] F. B. Arango and A. F. Koenderink, "Polarizability tensor retrieval for magnetic and plasmonic antenna design", *New J. Phys.* **15**, 073023 (2013), doi:10.1088/1367-2630/15/7/073023.

[169] I. M. Hancu, A. G. Curto, M. Castro-López, M. Kuttge and N. F. van Hulst, "Multipolar interference for directed light emission", *Nano Lett.* **14**, 166–171 (2014), doi:10.1021/nl403681g.

[170] A. G. Curto, T. H. Taminiau, G. Volpe, M. P. Kreuzer, R. Quidant and N. F. van Hulst, "Multipolar radiation of quantum emitters with nanowire optical antennas", *Nat. Commun.* **4**, 1750 (2013), doi:10.1038/ncomms2769.

[171] A. I. Kuznetsov, A. E. Miroshnichenko, Y. H. Fu, V. Viswanathan, M. Rahmani, V. Valuckas, Z. Y. Pan, Y. Kivshar, D. S. Pickard and B. Luk'yanchuk, "Split-ball resonator as a three-dimensional analogue of planar split-rings", *Nat. Commun.* **5**, 3104 (2014), doi:10.1038/ncomms4104.

[172] C. Rockstuhl, T. Zentgraf, E. Pshenay-Severin, J. Petschulat, A. Chipouline, J. Kuhl, T. Pertsch, H. Giessen and F. Lederer, "The origin of magnetic polarizability in metamaterials at optical frequencies - an electrodynamic approach", *Opt. Express* **15**, 8871–8883 (2007), doi:10.1364/OE.15.008871.

[173] S. A. Ramakrishna, "Physics of negative refractive index materials", *Rep. Prog. Phys.* **68**, 449 (2005), doi:10.1088/0034-4885/68/2/R06.

[174] T. Koschny, P. Markoš, D. R. Smith and C. M. Soukoulis, "Resonant and antiresonant frequency dependence of the effective parameters of metamaterials", *Phys. Rev. E* **68**, 065602 (2003), doi:10.1103/PhysRevE.68.065602.

[175] S. Varault, B. Rolly, G. Boudarham, G. Demésy, B. Stout and N. Bonod, "Multipolar effects on the dipolar polarizability of magneto-electric antennas", *Opt. Express* **21**, 16444–16454 (2013), doi:10.1364/OE.21.016444.

[176] T. Kaelberer, V. A. Fedotov, N. Papasimakis, D. P. Tsai and N. I. Zheludev, "Toroidal dipolar response in a metamaterial", *Science* **330**, 1510–1512 (2010), doi:10.1126/science.1197172.

[177] L. Mandel and E. Wolf, *Optical Coherence and Quantum Optics* (Cambridge University Press, Cambridge, 1995).

Publications

Publication I

P. Grahn, A. Shevchenko and M. Kaivola, “Electromagnetic multipole theory for optical nanomaterials”, *New Journal of Physics* **14**, 093033 (2012).

Publication II

P. Grahn, A. Shevchenko and M. Kaivola, “Interferometric description of optical metamaterials”, *New Journal of Physics* **15**, 113044 (2013).

Publication III

P. Grahn, A. Shevchenko and M. Kaivola, “Electric dipole-free interaction of visible light with pairs of subwavelength-size silver particles”, *Physical Review B* **86**, 035419 (2012).

Publication IV

P. Grahn, A. Shevchenko and M. Kaivola, “Multipole polarizability of a nanodimer in optical waves”, *Journal of the European Optical Society - Rapid Publications* **8**, 13009 (2013).

Publication V

P. Grahn, A. Shevchenko and M. Kaivola, “Theoretical description of bifacial optical nanomaterials”, *Optics Express* **21**, 23471–23485 (2013).

Aalto-DD 22/2014

ISBN 978-952-60-5576-3
ISBN 978-952-60-5577-0 (pdf)
ISSN-L 1799-4934
ISSN 1799-4934
ISSN 1799-4942 (pdf)

Aalto University
School of Science
Department of Applied Physics
www.aalto.fi

BUSINESS +
ECONOMY

ART +
DESIGN +
ARCHITECTURE

SCIENCE +
TECHNOLOGY

CROSSOVER

DOCTORAL
DISSERTATIONS